SYNTHESIS OF ZEOLITE SODIUM A AND X AND PREPARATION OF ZEOLITE-BIOMASS COMPOSITES FOR CARBON DIOXIDE ADSORPTION

RACHATA JAIKLA

A Thesis Submitted in Partial Fulfillment of the Requirements for the

Degree of Master of Science in Chemistry

Suranaree University of Technology

Academic Year 2024

การสังเคราะห์ซีโอไลต์โซเดียมเอและเอ็กซ์และการเตรียมคอมโพสิตของซีโอไลต์-ชีวมวลสำหรับการดูดซับคาร์บอนไดออกไซด์

นายรชฏ ใจกล้า

วิทยานิพนธ์นี้เป็นส่วนหนึ่งของการศึกษาตามหลักสูตรปริญญาวิทยาศาสตรมหาบัณฑิต
สาขาวิชาเคมี
มหาวิทยาลัยเทคโนโลยีสุรนารี
ปีการศึกษา 2567

SYNTHESIS OF ZEOLITE SODIUM A AND X AND PREPARATION OF ZEOLITE-BIOMASS COMPOSITES FOR CARBON DIOXIDE ADSORPTION

Suranaree University of Technology has approved this thesis submitted in partial fulfillment of the requirements for a Master's Degree.

Thesis Examining Committee

(Assoc. Prof. Dr. Sanchai Prayoonpokarach)
Chairperson

(Prof. Dr. Jatuporn Wittayakun)
Member (Thesis Advisor)

(Assoc. Prof. Dr. Theeranun Siritanon)
Member

(Asst. Prof. Dr. Sirinuch Loiha)
Member

(Assoc. Prof. Dr. Yupaporn Ruksakulpiwat)
Acting Vice Rector for Academic Affairs
and Quality Assurance

(Prof. Dr. Santi Maensiri)
Acting Dean of Institute of Science

รชฎ ใจกล้า : การสังเคราะห์ซีโอไลต์โซเดียมเอและเอ็กซ์และการเตรียมคอมโพสิตของซีโอไลต์-ชีวมวลสำหรับการดูดซับคาร์บอนไดออกไซด์ (SYNTHESIS OF ZEOLITE SODIUM A AND X AND PREPARATION OF ZEOLITE-BIOMASS COMPOSITES FOR CARBON DIOXIDE ADSORPTION) อาจารย์ที่ปรึกษา : ศาสตราจารย์ ดร.จตุพร วิทยาคุณ, 60 หน้า.

คำสำคัญ: ซีโอไลต์โซเดียมเอ / ซีโอไลต์โซเดียมเอ็กซ์ / LTA / FAU / ไฮโดรเทอร์มอล / การดูดซับก๊าซคาร์บอนไดออกไซด์

ซีโอไลต์ เช่น โซเดียมเอ (NaA) และโซเดียมเอ็กซ์ (NaX) เป็นวัสดุที่กันใช้อย่างแพร่หลายในทั้งกระบวนการเร่งปฏิกิริยา, การดูดซับ และการแยก อย่างไรก็ตามซีโอไลต์ที่อยู่ในรูปแบบผง มีความยุ่งยากต่อการใช้งาน ดังนั้นงานวิจัยนี้จึงได้เสนอการสังคราะห์ซีโอไลต์ โซเดียมเอ และ โซเดียมเอ็กซ์ คอมโพสิตกับชีวมวลอย่าง ไม้กระถินและตะเกียบไม้ไผ่ด้วยวิธี Dual Templating ซึ่งผลการวิเคราะห์ตัวอย่างด้วยเทคนิค XRD SEM และ TGA แสดงให้เห็นว่าซีโอไลต์สามารถก่อตัวภายในชีวมวลได้สำเร็จ แต่พบว่าปริมาณซีโอไลต์ภายในคอมโพสิตมีปริมาณที่น้อย ไม่เหมาะสมสำหรับการจะนำมาใช้ประโยชน์อย่างการการดูดซับก๊าซคาร์บอนไดออกไซด์ (CO_2) เพื่อแก้ไขปัญหาดังกล่าว งานวิจัยนี้จึงได้สังเคราะห์วัสดุคอมโพสิตชนิดใหม่ โดยใช้กระดาษที่ผลิตจากใบอ้อย คอมโพสิตกับซีโอไลต์โซเดียมเอและโซเดียมเอ็กซ์ ซึ่งวัสดุนี้แสดงความเป็นไปได้ที่จะนำมาใช้ประโยชน์ในงานด้านบรรจุภัณฑ์ เมื่อวิเคราะห์ด้วยเทคนิค XRD, SEM, TGA และการดูดซับไนโตรเจน พบว่าคอมโพสิตจากกระดาษมีปริมาณซีโอไลต์มากกว่าคอมโพสิตจากไม้ โดยคอมโพสิตโซเดียมเอแสดงของการดูดซับไอโซเทอร์มแบบที่ II ในขณะที่ โซเดียมเอ็กซ์ แสดงไอโซเทอร์มของการดูดซับแบบที่ I ซึ่งแสดงให้เห็นถึงความแตกต่างของโครงสร้างรูพรุนในวัสดุทั้งสองชนิด จากการศึกษาการดูดซับก๊าซคาร์บอนไดออกไซด์ พบว่าคอมโพสิตโซเดียมเอ มีความสามารถในการดูดซับได้มากที่สุด (1.25 mmol/g) เนื่องมาจากคอมโพสิตโซเดียมเอ มีปริมาณซีโอโลต์ที่มากกว่า ทั้งนี้ผลการวิเคราะห์ไอโซเทอร์ม พบว่าพฤติกรรมการดูดซับของคอมโพสิตมีความสอดคล้องกับแบบจำลอง Langmuir–Freundlich สำหรับการดูดซับเอทิลีนที่ศึกษาโดยใช้เทคนิค Ethylene-TPD แสดงให้เห็นว่ามีเพียงคอมโพสิตโซเดียมเอเท่านั้นที่เหมาะสมกับการดูดซับ เนื่องจากสามารถดูดซับที่ช่วงอุณหภูมิต่ำกว่า 200 °C ในขณะที่คอมโพสิตโซเดียมเอ็กซ์ไม่สามารถดูดซับในช่วงดังกล่าว

สาขาวิชาเคมี ลายมือชื่อนักศึกษา รชฎ ใจกล้า

ปีการศึกษา 2567 ลายมือชื่ออาจารย์ที่ปรึกษา จตุพร วิทยาคุณ

RACHATA JAIKLA : SYNTHESIS OF ZEOLITE SODIUM A AND X AND PREPARATION OF ZEOLITE-BIOMASS COMPOSITES FOR CARBON DIOXIDE ADSORPTION. THESIS ADVISOR : PROF. JATUPORN WITTAYAKUN, Ph.D. 60 PP.

Keyword: ZEOLITE SODIUM A/ ZEOLITE SODIUM X/ LTA/ FAU/ HYDROTHERMAL/ CARDONDIOXIDE ADSORPTION

Zeolites such as sodium A (NaA) and sodium X (NaX) are widely used in catalysis, adsorption and separation. However, their powder form can be difficult to handle in practical applications. This study synthesizes NaA and NaX zeolites embedded in biomass materials—lead tree wood and bamboo chopsticks—using a dual templating method. Characterization by XRD, SEM, and TGA confirmed successful synthesis, but revealed low zeolite content, making these composites unsuitable for applications such as carbon dioxide (CO_2) adsorption. To overcome this limitation, alternative composites were developed using paper made from sugarcane leaves, combined with NaA and NaX zeolites. These materials, suitable for potential packaging applications, were characterized using XRD, SEM, TGA, and nitrogen adsorption. The results showed significantly higher zeolite content than wood-based composites. NaA composites exhibited type II isotherms, while NaX composites showed type I isotherms, indicating their respective pore structures. CO_2 adsorption studies revealed that NaA composites had the highest adsorption capacity (1.25 mmol/g), attributed to higher zeolite content. Isotherm analysis followed the Langmuir–Freundlich model. Ethylene adsorption studied using the ethylene-TPD technique showed that only composite NaA was suitable for adsorption, as it could adsorb ethylene at temperatures below 200 °C, whereas composite NaX could not adsorb in this temperature range.

School of Chemistry

Academic Year 2024

Student's Signature _____

Advisor's Signature _____

ACKNOWLEDGEMENTS

I would like to express my deepest gratitude to Prof. Dr. Jatuporn Wittayakun, my thesis advisor, for his invaluable support, guidance, and encouragement throughout the past three years. His expertise and mentorship have been instrumental in the completion of this research.

I sincerely acknowledge the financial support provided by Suranaree University of Technology (SUT) through my scholarship. Special thanks to the staff at The Center for Scientific and Technological Equipment for their assistance and technical support during the research process.

Finally, I would like to extend my appreciation to the members of the Catalysis Group at SUT for their valuable advice and discussions, which have greatly contributed to the success of this thesis.

Rachata Jaikla

CONTENTS

CONTENTS (Continued)

LIST OF TABLES

LIST OF FIGURES

LIST OF FIGURES (Continued)

CHAPTER I

INTRODUCTION

The global challenge of climate change has accelerated the need for effective solutions to mitigate the growing concentration of carbon dioxide (CO_2) in the atmosphere. As CO_2 emissions continue to rise, it is imperative to explore innovative materials and techniques for its capture and sequestration. One promising avenue of research in this regard is the utilization of zeolite-biomass composites for CO_2 adsorption.

Zeolite is a crystalline aluminosilicate compound with the molecular formula $Na_x[(AlO_2)_x(SiO_2)_y]{\cdot}nH_2O$. It possesses a three-dimensional structure composed of silicate $[(SiO_4)^{4-}]$ and aluminate $[(AlO_4)^{5-}]$ units interconnected through four oxygen atoms, with shared oxygen between silicate and aluminate species. Zeolites NaA and NaX have been chosen as the primary targets for synthesis due to their relative ease of production compared to other zeolite types. NaA exhibits superior selectivity for CO_2 adsorption compared to zeolite Na-CHA-4 and Na-ZSM-5 (Couck et al., 2017; Guo et al., 2018), making it an excellent choice for capturing this greenhouse gas from gaseous mixtures. On the other hand, zeolite NaX excels in terms of its capacity to adsorb CO_2, which is better than zeolite NaY, Na-RHO, and Na-MER (Dabbawala et al., 2020; Georgieva et al., 2019; Lozinska et al., 2014). This ensures efficient gas sorption.

The effectiveness of zeolite NaX in CO_2 adsorption is further highlighted by its successful use in enhancing porous carbon, as demonstrated by Gan et al. (2021). In their study, they synthesized zeolite NaX composites with activated carbon from rice husk, showcasing high CO_2 adsorption capacity and selectivity, along with excellent regeneration ability. However, rice husk is a fragile and easily degradable plant material under simple laboratory operations. To address this issue, the use of hardwood, such as Thailand's abundant Lead tree wood, serves as a suitable support, while bamboo chopsticks, a waste product from the food industry, offer an eco-friendly and cost-effective option. By synthesizing zeolite-biomass composites using a method used by

Valtchev et al. (2004a), called dual templating, biomass is added to the zeolite precursor and subjected to a hydrothermal process to produce zeolite composites with biomass. Additionally, relevant research by Krukkratoke et al. (2022) showed the potential of NaY/lead tree wood composites for Ni(II) adsorption, while Tawachkultanadilok et al. (2023) demonstrated the efficacy of NaY/bamboo composites for the same purpose, underlining the suitability of biomass-based composites for environmental remediation. However, these materials have not yet been used in CO_2 adsorption. In addition, both studies show that synthesizing NaY in raw wood can lead to NaP impurities, which can be mitigated by using refluxed wood or by synthesizing alternative zeolites like NaA and NaX.

Recent research on composite materials by Krukkratoke et al. (2022) has demonstrated that composites synthesized using the dual templating method result in materials containing only small amounts of zeolite (12.4%–22.4%). An interesting alternative method to produce composites with higher zeolite content involves incorporating pre-synthesized zeolite powder into pulp, which is subsequently transformed into a paper composite. Additionally, various biomass sources, such as sugarcane leaves (Minja et al., 2021) , can be used in paper production as a sustainable alternative to burning, thereby helping to reduce CO_2 emissions. Paper/zeolite composites can also be used in packaging applications for produce, such as fruit, to adsorb ethylene and slow down ripening (do Nascimento Sousa et al. (2020).

1.1 Objectives

The objectives of this thesis are: (i) to utilize biomass by synthesizing a composite material of zeolite (NaA or NaX) with biomass (lead tree wood, bamboo chopsticks and paper made from sugarcane leaves), (ii) to conduct a comprehensive analysis of the composition and properties of zeolite composites with biomass materials and (iii) to utilize composites with biomass as effective adsorbents for CO_2 and ethylene.

CHAPTER II

LITERATURE REVIEW

This chapter provides a literature review on the fundamentals of biomass materials, CO_2 and ethylene capture using zeolites, and the synthesis of zeolite/biomass composites.

2.1 Biomass materials

2.1.1 Lead tree wood

Leucaena leucocephala, commonly known as the Lead tree, is native to Southern Mexico and Northern Central America. It has since spread to various tropical and subtropical regions, including the abundant presence of the Lead tree in Nakhon Ratchasima province. Belonging to the family Fabaceae, it is a remarkably fast-growing plant. This shrub or small tree can reach 3-10 meters and is classified as non-deciduous (Sharma et al., 2022).

The Lead tree has gained global recognition for its use as animal feed due to its longevity and high nutritional value. Additionally, it serves multiple purposes such as firewood production, timber, human consumption, green manure, shade provision, and erosion control. Moreover, the Lead tree possesses various pharmacological properties, making it valuable for medicinal purposes (Zayed et al., 2018). However, as the Lead tree grows rapidly, farmers often cut and burn excess plants when their cultivation exceeds human needs.

Lead tree wood consists of cellulose (55.87%), hemicellulose (34.73%), and lignin (18.63%) (Hazim et al., 2017). The Lead tree is a dicotyledon plant with a wide diameter of xylem and phloem, approximately 10 μm, which is wider than zeolite NaA (3-12 μm) (Loiola et al., 2012) and zeolite NaX (10-20 μm) (Iftitahiyah et al., 2018).

Lead tree wood can be used to synthesize activated carbon with a surface area of 590 m^2/g, a pore volume of 0.27 cm^3/g, and a pore width of 1.85 nm. This corresponds to a 70% microporosity with a well-developed porous structure and the ability to adsorb CO_2 at 40.54 cm^3/g at 25°C and 1 atm (Gautam et al., 2023).

2.1.2 Bamboo chopsticks

Disposable bamboo chopsticks (DBCs) are extensively used in various East and Southeast Asian countries, including Thailand, due to their convenience and affordability. China, where chopsticks originated, has reported an annual usage rate of approximately 80 billion pairs of DBCs, leading to the deforestation of around 20 million of 20-year-old trees each year. While data specific to Thailand's DBC consumption and production quantities are lacking, it is evident that DBCs have become a significant issue for municipal waste management. When disposed of with other garbage in plastic bags, DBCs puncture the bags, causing spillage and complicating waste collection efforts (Jodnok et al., 2021).

DBCs consist mainly of carbon (62.26% wt), followed by oxygen (43.73% wt) and potassium (1.41% wt). DBCs have an average pore size of 6.583 nm, classified as mesoporous (Wijitkosum, 2023), which is wider than zeolite NaA and NaX. Bamboo can be used to synthesize activated carbon with a surface area of 561.1 m^2/g and the ability to adsorb CO_2 at a rate of 74.46 mg/g at 25°C and 1 atm (Koo-amornpattana et al., 2022).

2.1.3 Paper from sugarcane leaves

Hardwood has traditionally been the primary source of cellulosic fibers for the pulp and paper industry. However, the increasing demand for hardwood has led to significant environmental concerns, including deforestation, ecological imbalances, and climate change. In response, there has been growing interest in alternative fiber sources, such as grass (Lee et al., 2022) and plant leaves (Adeoye et al., 2021). One particularly promising alternative fiber source is sugarcane waste.

Sugarcane (*Saccharum officinarum*) originates from Southeast Asia and New Guinea (Lebot, 1999) and is an important economic crop in Thailand. The majority of Thailand’s sugarcane production is consumed domestically, with the remainder

exported to the global market. Thailand ranks as the world's fifth-largest sugar exporter, producing approximately 60–80 million tons of sugarcane annually (Chokwarakul, 2018). Sugarcane harvesting is typically conducted using two methods: cutting fresh sugarcane or burning it before cutting. The burning method is widely used by farmers due to labor shortages and the convenience of harvesting. However, this method significantly impacts the environment, contributing to air pollution, soil degradation, and the greenhouse effect. Additionally, it directly affects the quality of the harvested sugarcane (Kawon et al., 2022). The sugarcane industry generates substantial waste, primarily in the form of sugarcane leaves and bagasse. Among these, sugarcane bagasse is widely used in the paper industry, accounting for approximately 2–5% of global pulp and paper production (Rainey and Covey, 2016). Sugarcane leaves have also been successfully utilized in papermaking (Minja et al., 2021).

During the pulping process in paper production, delignification is typically carried out using chemical treatments such as sodium hydroxide (NaOH) (Minja et al., 2021). Additionally, zeolite powder can be incorporated into the pulp to produce a zeolite/paper composite, enhancing the properties of the final paper product.

2.2 CO_2 Capture using zeolites

The quest for effective CO_2 capture materials has led to the exploration of a variety of adsorbent classes, including carbon-based materials, metal-organic frameworks (MOFs), and zeolites. Each of these materials possesses distinct advantages and limitations, making them suitable for different applications within the field of gas separation.

Carbon-based materials are appealing due to their cost-effectiveness, thermal stability, and hydrophobic nature. However, their relatively weak CO_2 interaction limits adsorption capacity and selectivity at low pressures. Doping with heteroatoms can enhance CO_2 interaction but increases hydrophilicity (Choi et al., 2009). MOFs, known for their high specific surface areas, offer impressive CO_2 adsorption capacities, primarily at high pressures. Their weaker CO_2 interaction makes them less suitable for lower-pressure applications, and they face challenges in terms of cost, hydrothermal stability, and regeneration (Millward and Yaghi, 2005).

Despite these challenges, zeolites stand out as a promising class of adsorbents due to their stability, cost-effectiveness, and the ability to fine-tune their physicochemical properties to optimize adsorption behavior. This adaptability includes adjusting pore size, organization, and composition to enhance their suitability for CO_2 separation, making zeolites an attractive option for separating CO_2 from other gases like CH_4 or N_2 (Boer et al., 2023).

One key factor influencing CO_2 adsorption by zeolites is the presence of basic sites. Zeolites are composed of a framework of tetrahedral TO_4 units (T = Si or Al), interconnected through shared oxygen atoms. When Si^{4+} is substituted with Al^{3+}, a net negative charge is introduced, which is balanced by Na^+ cations. These Na^+ ions and the negatively charged framework sites act as active basic sites for CO_2 adsorption. A lower Si/Al ratio (i.e., higher Al content) and a higher Na/Si ratio are associated with increased basicity, leading to enhanced CO_2 adsorption capacity (Keawkumay et al., 2024). Furthermore, smaller zeolite crystal sizes contribute to higher adsorption capacity and faster CO_2 uptake at lower pressures. The use of purer precursors, such as high-purity aluminum sources, also improves crystallinity, optimizes surface acidity, and enhances surface functionality (Keawkumay et al., 2025).

The ability of zeolites to adsorb CO_2 can also be utilized in packaging applications, as CO_2 is one of the gases released by fruits and vegetables. Excessive carbon dioxide can seriously damage the skin and flesh of the fruit (Krupa and Tomala, 2021).

Among these zeolites, NaA and NaX types are easier to synthesize compared to other zeolites. Table 1 displays examples of sodium zeolite in terms of adsorption capacity and CO_2 selectivity. Zeolite NaA is a structured zeolite known as Linde Type A (LTA), with an 11.4 Å diameter supercage connected by eight-ring openings and a 4.1 Å diameter cavity (McCusker and Baerlocher, 2001). Zeolite NaX is a zeolite with a structure referred to as Faujasite (FAU) and a silicon-to-aluminum ratio of 1 to 1.5. Zeolite NaX structures have a 1.24 nm (12.4 Å) diameter supercage connected by twelve-ring openings and a 0.74 nm (7.4 Å) diameter cavity (Du, 2013). Zeolite NaA, with its smaller pore size, shows promising enhanced selectivity, while zeolite NaX, with its larger pore size, was chosen for its potential to provide greater CO_2 adsorption capacity (Boer et al., 2023).

Table 2.1 Example of the Sodium Zeolites Adsorption Capacity and CO_2 Selectivity.

Material	Si/Al	Adsorption condition		nCO_2 (mmol/g)	Pure Sel. CO_2/N_2	N_2 Pure Sel. CO_2/CH_4	REF.
		Pressure (bar)	Temp. (°C)				
NaA	1[a]	0.85	25	3.9	13		Liu et al., 2010
NaX	1	1	25	6.3		8	Moura et al., 2016
NaY	2.2	1	25	4.7			Dabbawala et al., 2020
Na-BEA	7.4	1	25	2.7	17		Yang et al., 2010
Na-RHO	3.9	1	25	4.9		49	Lozinska et al., 2014
Na-CHA-4	4	1	25	4.7	7	4	Guo et al., 2018
Na-MER	3.8	1	25	3.8		13	Georgieva et al., 2019
Na-ZSM-5	25	1	30	2.1	8	3	Couck et al., 2017

[a] The Si/Al ratio was not measured, but zeolite A always has a Si/Al ratio of 1.

When compared to other sodium zeolites, NaY and Na-CHA-4 have pore sizes between those of NaA and NaX, resulting in adsorption capacities higher than zeolite NaA but lower than NaX. The higher selectivity of Na-BEA is due to its smaller pore size, even smaller than zeolite NaA. On the other hand, Na-RHO exhibits higher capacity and selectivity, thanks to a unique trapdoor mechanism enabled by the thermal motion of cations. This mechanism allows CO_2 to enter its small pores and interact with the zeolite framework, while CH4 is prevented from entering, leading to enhanced CO_2 adsorption performance. Additionally, Na-ZSM-5 shows lower capacity and

selectivity due to limited interaction, in which CO_2 interacts only with the Na+ sites located in the 10-member ring channel (Boer et al., 2023).

Zeolite can also be used to synthesize supported materials, such as biomass. In previous research conducted by Gan et al. (2021), they synthesized zeolite NaX with activated carbon derived from rice husk. This synthesis has been shown to enhance the CO_2 adsorption capacity from 1.05 to 1.48 mmol/g and the selectivity from 6.91 to 10.52 when compared to their activated carbon counterpart.

Additional research by Tawachkultanadilok et al. (2024) synthesized micro- and nano-sized NaY zeolite supported on bamboo charcoal. While the overall composite exhibited lower CO_2 adsorption than pure zeolite, a comparison based solely on the zeolite content revealed that both micro- and nano-sized NaY in the composites showed significantly higher adsorption capacities than pure NaY zeolite (micro: 6.67 mmol/g vs. 1.59 mmol/g, nano: 14.82 mmol/g vs. 2.70 mmol/g). This demonstrates that dispersing NaY zeolite on bamboo charcoal enhances CO_2 uptake per unit weight of zeolite.

2.3 Ethylene Capture using Zeolites

Ethylene (C_2H_4), even at trace concentrations, plays a crucial role in the ripening and senescence of fruits and vegetables. Its presence can either benefit or negatively impact postharvest quality, depending on the type and sensitivity of the produce. Controlling ethylene is essential for reducing postharvest losses (Domínguez et al., 2016).

As a volatile organic compound (VOC), ethylene regulates plant growth and development by increasing respiratory activity, thereby accelerating metabolism. It is biologically active at extremely low concentrations (in the ppb range) (Keller et al., 2013). During preharvest, ethylene mediates responses to biotic and abiotic stress (Guan et al., 2015; Kazan, 2015). Postharvest, it is often used to standardize ripening, especially for climacteric fruits like bananas and tomatoes (Seymour et al., 2013), but may also accelerate spoilage in sensitive produce by inducing yellowing, softening, and senescence (Cherian et al., 2014; Dhall, 2013).

Zeolites are one of the most studied materials for ethylene adsorption due to their high surface area, tunable pore size, and ion-exchange capacity. Other materials such as clays, silica, alumina, and activated carbon have also been explored (Álvarez-Hernández et al., 2018). Often, these adsorbents are combined with oxidizing agents like $KMnO_4$ to enhance ethylene capture efficiency. However, $KMnO_4$ is toxic and must be isolated from direct contact with food, typically by embedding in sachets or films (Vermeiren et al., 1999).

Table 2.2 Example of the zeolites-based materials for adsorption of ethylene.

Material	Adsorption condition		nEthylene (mmol/g)	Reference
	Pressure (bar)	Temperature (℃)		
Chitosan/Clinoptilolite composites	0.5	25	7.7×10^{-1}	do Nascimento Sousa et al. (2020)
4A zeolite	1	25	2.3	Min et al. (2020)
5A zeolite	1	25	2.5	Min et al. (2020)
13X zeolite	0.4	25	2.5	Costa et al. (1991)
13X zeolite	0.4	25	2.5	Hyun and Danner (1982)

Table 2.2 presents examples of zeolite-based materials used for ethylene adsorption. Many studies on ethylene adsorption have utilized natural zeolites, such as clinoptilolite. For instance, do Nascimento Sousa et al. (2020) synthesized chitosan/clinoptilolite composites, where chitosan—commonly used in packaging films—was combined with clinoptilolite as a non-toxic alternative to $KMnO_4$ for ethylene adsorption. The composite exhibited an ethylene adsorption capacity of 7.7×10^{-1} mmol/g at 25℃.

Other studies have utilized commercial zeolites such as zeolite A and zeolite X. Although these materials are more expensive than natural zeolites, they exhibit significantly higher ethylene adsorption capacities. For example, Min et al. (2020) reported that zeolite A adsorbed 2.3 mmol/g in 4A zeolite and 2.5 mmol/g in 5A zeolite. Similarly, studies on zeolite X showed ethylene adsorption capacities of 2.5 mmol/g for 13X zeolite (Costa et al., 1991; Hyun and Danner, 1982). These findings highlight the strong potential of zeolite A and zeolite X for incorporation into food packaging for effective ethylene removal.

2.3 Synthesis of zeolite/biomass composite

The synthesis of zeolite/wood composites represents a fascinating approach to enhance the material properties and application potential of zeolites. This method allows materials to grow within the vascular systems of various plant templates, leading to innovative advances in zeolite synthesis. Over the past two decades, several notable examples have emerged within this field, primarily focusing on ZSM-5 zeolite composites with plant parts, such as leaves and stems of Equisetum arvense (Valtchev et al., 2004b), stems of corn (Krishnamurthy et al., 2016), and rice husk (Morawala et al., 2019).

Table 2.3 shows examples of the material/wood composite synthesis. Among these, ZSM-5 zeolite synthesized using plant templates exhibited exceptional promise. For instance, the use of Equisetum arvense, a fragile and easily degradable plant, highlighted the need for robust plant templates to enhance the efficiency of the resulting material. Corn stems, on the other hand, provided tangible pellets that appeared ready for use, offering a clear advantage in terms of convenience.

When exploring the synthesis of zeolites, such as zeolite NaA and NaX, an interesting observation is the lack of reports concerning their synthesis using plant templates. Notably, Tepamat et al. (2013) attempted to synthesize NaA and Gan et al. (2021) with zeolite NaX, both groups prepared activated carbon composites derived from rice husks, providing a sustainable and cost-effective means of synthesizing these materials.

A common thread among these diverse approaches to zeolite/wood composite synthesis involves mixing ingredients with a wood template. Subsequently, the mixture is subjected to hydrothermal treatments under varying conditions, such as temperature, time, refluxing, and aging. This method has been successfully applied across various plant templates and solid substrates, leading to the production of zeolite composites with unique properties (Gan et al., 2021; Krishnamurthy et al., 2016; Morawala et al., 2019; Valtchev et al., 2004b).

Table 2.3 Examples of the material/wood composite synthesis.

Material	Supporting material		Surface area (m^2/g)	Application	Reference
	Name	Type			
ZSM-5	Equisetum arvense	Leaves and stems	47		Valtchev et al., 2004
ZSM-5	Corn	Stems	226	Esterification of benzyl alcohol with hexanoic acid	Krishnamurthy et al., 2016
ZSM-5	Rice	Husk	328	Synthesis of n-butyl levulinate	Morawala et al., 2019
NaA	Rice	Husk	64.60		Tepamat et al., (2013)
NaX	Rice	Husk	980.8	CO_2 adsorption	Gan et al., 2021
NaY	Lead tree	Wood	45	Ni (II) adsorption	Krukkratoke et al., 2022
NaY	Bamboo	Wood	16.1	Ni (II) adsorption	Tawachkultanadilok et al., 2023

Another notable method for biomass/zeolite synthesis, aside from the dual templating approach by Izadyar and Fatemi (2013), involves incorporating zeolite 13X-based powder into wood pulp before transforming it into paper/zeolite composites. This method offers an alternative approach compared to the work of Krukkratoke et al. (2022), who created composites with a zeolite content of approximately 12–22%.

Although various templates have been used in zeolite composite synthesis, the combination of zeolite NaA and NaX with wood and paper remains largely unexplored. With their high surface area and stability, these zeolites show great potential for catalysis, separation, and adsorption. Further research could lead to novel materials with enhanced properties.

CHAPTER III

EXPERIMENTAL

3.1 Chemicals

The Lead tree wood used in the synthesis was obtained from the area around the Center for Scientific and Technological Equipment Building 2 (F2) of Suranaree University of Technology (Nakhon Ratchasima, Thailand). Bamboo chopsticks were commonly available at 7-Eleven stores, and sugarcane leaves were collected from sugarcane fields around Suranaree University of Technology (Nakhon Ratchasima, Thailand). The chemicals used for biomass activation and the synthesis of zeolite NaA and NaX included silica fumed (SiO_2) (99.8% SiO_2, Sigma-Aldrich), sodium aluminate ($NaAl_2O_3$) (50–56% Al_2O_3, 37–45% Na_2O, Sigma-Aldrich) and sodium hydroxide (NaOH) (97% wt NaOH, Carlo Erba).

3.2 Synthesis of zeolite NaA and NaX

3.2.1 Synthesis of zeolite NaA

Zeolite NaA was synthesized from a gel composition of $6Na_2O$: Al_2O_3: SiO_2: $150H_2O$, following the procedure outlined by Khaosomboon et al. (2018). 90 mL of DI water was measured into a 250 mL polypropylene (PP) bottle. Gradually, 12.27 g of sodium hydroxide pellets (weighed using a plastic beaker) were added, dividing them equally into another 250 mL PP bottle. The first part of the solution was mixed with 6.3552 g of sodium aluminate. In the second part of the solution, 2 g of silica was added and stirred with a magnetic bar at 90°C for 3 hours. Both parts of the solution were then mixed and stirred for 30 minutes. To prevent water evaporation during zeolite gel crystallization, tape was applied tightly between the area where the bottle and the cap meet. Crystallization was conducted at 80°C for 2.5 hours in a hot air oven. After cooling, the white precipitate (synthesized zeolite NaA) was washed with distilled water and centrifuged at 4,000 rpm for 4 minutes until the pH was lower than 9.

The PP bottle cap was removed, and the mouth of the PP bottle was covered with a pre-punctured aluminum foil sheet to allow water to evaporate. Then, the synthesized NaA zeolite powder was dried overnight at 90°C in a hot air oven.

3.2.2 Synthesis of zeolite NaX

Zeolite NaX was synthesized from a gel composition of $NaAlO_2$: $4SiO_2$: 16NaOH: $88H_2O$, following the procedure described by (Jantarit et al., 2020). To obtain a larger amount of zeolite NaX, three times more substrates were used. A sodium silicate solution was prepared by pouring 26.76 g of DI water into a 250 mL polypropylene (PP) bottle. Gradually, 4.83 g of sodium hydroxide pellets (weighed using a plastic beaker) was added, followed by the addition of 12.3 g of silica. This mixture was stirred with a magnetic bar for 18 hours at room temperature. For the sodium aluminate solution, 264 g of DI water was weighed into a 500 mL PP bottle. Gradually, 27.24 g of sodium hydroxide pellets were added, followed by the addition of 4.08 g of sodium aluminate, and the mixture was stirred for 1 hour. The sodium silicate solution was then mixed with the sodium aluminate solution in a 500 mL PP bottle and stirred for 1 hour. To prevent water evaporation during zeolite gel crystallization, tape was tightly applied between the area where the bottle and the cap meet. Crystallization was carried out at 90°C for 18 hours in a hot air oven. After cooling, the white precipitate (synthesized zeolite NaX) was washed with distilled water and centrifuged at 4,000 rpm for 4 minutes until the pH is around 7.

The PP bottle cap was removed, and the mouth of the PP bottle was covered with a pre-punctured aluminum foil sheet to allow water to evaporate. Then, the synthesized NaX zeolite powder was dried overnight at 90°C in a hot air oven.

3.3 Synthesis of zeolite/biomass composite

3.3.1 Preparation of Lead tree wood and Bamboo chopstick

The lead tree wood was cut to a diameter of 0.75 cm and a height of 0.5 cm, while the bamboo chopsticks were cut to a length of 0.5 cm. The lead tree wood sample was named LTW, while the bamboo chopstick sample was named BW.

3.3.2 Synthesis of NaA and NaX Composites with LTW and BW

In the synthesis of zeolite NaA in biomass, zeolite NaA was prepared using the same procedure as described above, but 2 g of lead tree wood or bamboo chopstick was added to the second part of the solution before the addition of silica. Similarly, for the synthesis of zeolite NaX in biomass, 2 g of lead tree wood or bamboo chopstick was added to the solution during the preparation of the sodium aluminate solution, before the addition of sodium aluminate.

In both synthesis processes, after the addition of lead tree wood or bamboo chopstick, the mixture was aged for 24 hours. Following crystallization, the zeolite–biomass composites were filtered and washed using a sonication method at 40°C for 5 minutes, while the powders were washed by centrifugation at 4000 rpm for 5 minutes. Both the composites and powders were washed several times by sonication or centrifugation with deionized water until the pH of the samples reached approximately 7. Subsequently, the composites and powders were dried at 90°C overnight in a hot air oven to obtain zeolite/wood composites.

The lead tree wood/zeolite composite samples were named LTW-NaA and LTW-NaX, while the bamboo chopstick/zeolite composites were named BW-NaA and BW-NaX. Finally, the powder samples formed outside the wood during the synthesis of the lead tree wood/zeolite composites were named LTW-NaA-P and LTW-NaX-P, while those formed outside the bamboo chopstick/zeolite composites were named BW-NaA-P and BW-NaX-P.

3.3.3 Synthesis of NaA and NaX Composites with SLP

Paper made from sugarcane leaves was synthesized using the method described by Rani et al. (2018). First, 10 g of sugarcane leaves were blended into very small pieces and then added to a 10% NaOH solution at a 1:1 weight ratio of NaOH to sugarcane leaves. The mixture was heated at 80°C for 4 hours to convert the sugarcane leaves into pulp, and then washed three times with deionized water. The resulting pulp was poured onto a deckle, spread evenly, and dried overnight in a fume hood to obtain paper.

For the synthesis of the zeolite/paper composite, zeolite powder synthesized from a previous method was added to the pulp after washing with DI water, using a 1:2 ratio of sugarcane leaves to zeolite. The mixture was stirred for 30 minutes and then transferred to a fume hood for drying. The sugarcane paper sample without zeolite was named SLP, while the sugarcane paper/zeolite composites were named SLP-NaA and SLP-NaX

3.4 Material characterization

The phases of the composites were analyzed using X-ray diffraction (XRD) on a Bruker D8 ADVANCE instrument with Cu K_α radiation, operating at a voltage and current of 40 kV and 30 mA. The scan speed was set at 0.2 s/step, and the increment was 0.02 s/step.

The morphology and elemental analysis of the composites was examined via scanning electron microscopy with energy dispersive X-ray spectroscopy (SEM-EDS, Carl Zeiss, Auriga® series, Carl Zeiss NTS GmbH, Oberkochen, Germany) with an accelerating voltage of 30 kV. The samples were spread on silver paint and coated with gold using sputtering.

The thermal decomposition of the wood composites was investigated through thermogravimetric analysis (TGA) on a Mettler Toledo model TGA/DSC1 (Mettler Toledo AG, Analytical, Schwerzenbach, Switzerland) under an air-zero atmosphere. The gas flow rate was 50 mL/min, and the heating rate was 10°C/min up to 800°C. Following the combustion of the wood, the remaining residues were assumed to primarily consist of zeolite.

Nitrogen adsorption isotherms of the composites were obtained using a Quantachrome Instruments, Autosorb IQ series (Micromeritics, USA) at liquid nitrogen temperature. Prior to the measurement, the samples were degassed at 70°C for 24 hours. The specific surface areas (SBET) were calculated using the Brunauer-Emmett-Teller (BET) equation.

3.5 CO_2 and ethylene adsorption application

Samples were studied for the adsorption of CO_2 using the BELSORP MAX X Analyzer, following the procedure described by Madhu et al. (2022). Before the analysis, the samples were degassed at 150°C for 12 hours. The operating temperature during the measurement of CO_2 adsorption was 25°C with a range of 0-100 kPa. Then, the amount of CO_2 absorbed was plotted against pressure.

An ethylene adsorption application study was conducted using ethylene temperature-programmed desorption (ethylene-TPD), following the modified procedure outlined by Roy et al. (2023). To begin, 0.05 g of the sample was packed into the sample cell and topped with quartz wool. The sample was heated at a rate of 10°C/min under a flow of helium (He) from room temperature to 200°C and held at this temperature for 30 minutes. After cooling to 50°C, ethylene diluted with inert gas (7.5% C_2H_4/He) was introduced at a rate of 30 ml/min for 30 minutes. Subsequently, the sample was purged with He for 30 minutes to remove physiosorbed species. The temperature was ramped at 10°C/min from 100 to 810°C. The amount of ethylene desorbed versus time was recorded, and the TPD profile was compared with a no-gas TPD (in which He was fed instead of 7.5% C_2H_4/He). The total amount of ethylene desorbed was determined by integrating the area under the curve.

CHAPTER IV

RESULTS AND DISCUSSION

4.1 Characterization of wood composites

4.1.1 XRD pattern and SEM images of wood composites

Lead tree wood (LTW) and bamboo chopsticks (BW) were analyzed using XRD, SEM and TGA. Figure 4.1 presents the XRD patterns of LTW (Figure 4.1a) and BW (Figure 4.1b). The XRD patterns display two broad peaks at 14° and 22°, indicating that these structures are amorphous, with peak positions similar to those of cellulose crystals (Li et al., 2011). Additionally, both LTW and BW show a pattern consistent with calcite (according to the RUFF database: calcite R050128), suggesting the presence of impurities in both materials.

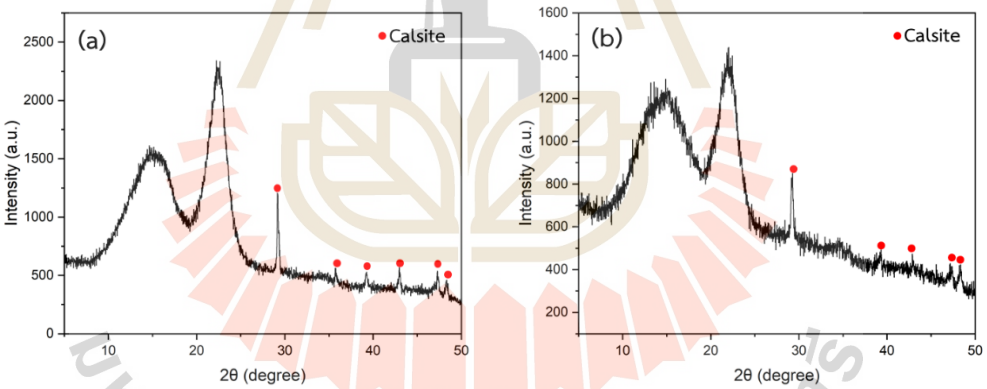

Figure 4.1 XRD pattern of LTW (a) and BW (b).

Figure 4.2 presents the SEM images of dissected LTW (4.2a, 4.2b, 4.2c) and BW (4.2d, 4.2e, 4.2f) at different magnifications. Figure 4.2a reveals the vascular structure of LTW with a pore width of approximately 10 μm, which was consistent with the findings of Krukkratoke et al. (2022). Similarly, Figure 4.2d shows that BW had a pore size of around 12 μm. Additionally, Figures 4.2b, 4.2c, 4.2e, and 4.2f indicate that both LTW and BW had rough surfaces.

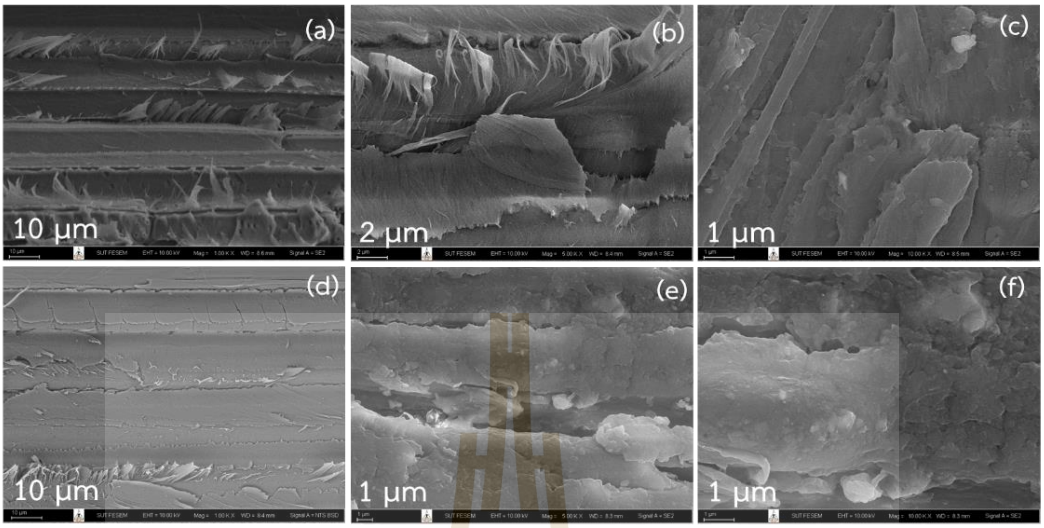

Figure 4.2 SEM images with different magnifications of LTW (a) 1000x (b) 5000x (c) 10000x and BW (d) 1000x (e) 5000x (f) 10000x.

4.1.2 XRD pattern and SEM images of zeolite composites with wood

Figure 4.3 presents the XRD patterns of LTW composites with zeolite NaA (LTW-NaA) and zeolite NaX (LTW-NaX), compared to LTW, zeolite NaA (Pluth and Smith, 1980), and zeolite NaX (Olson, 1995). Figure 4.3a shows that LTW-NaA exhibited less intense broad peaks at 14° and 22°, indicating a partial loss of cellulose structure. Additionally, LTW-NaA displaya characteristic peaks of zeolite NaA, suggesting that zeolite NaA had grown onto the LTW surface in sufficient quantity for its peaks to be detected. In contrast, Figure 4.3b shows that LTW-NaX did not exhibit clear peaks of zeolite NaX, indicating that either zeolite NaX had not grown or had formed in very low quantities on the LTW surface. This suggested that zeolite NaA adhered more effectively to the biomass surface compared to zeolite NaX. Lastly, the peak at 29° confirmed the presence of calcite impurities in both composites; however, LTW-NaX exhibited a weaker peak, likely due to the longer crystallization time of zeolite NaX.

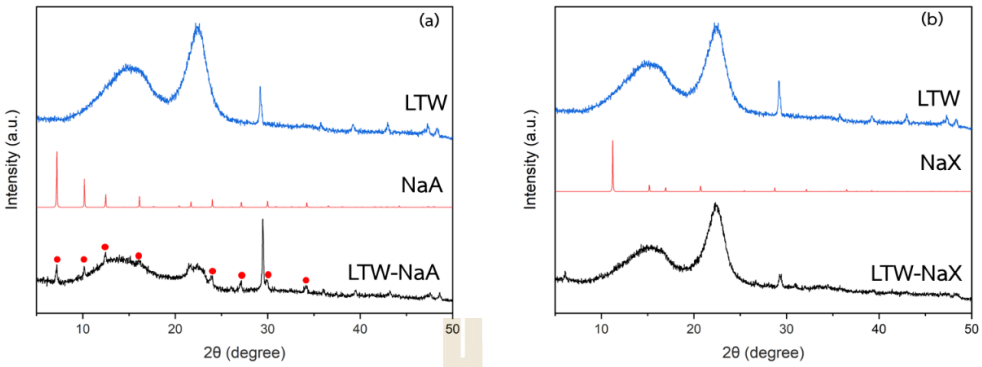

Figure 4.3 XRD pattern of LTW (blue line), zeolite (red line: NaA (a) (Pluth and Smith, 1980), NaX (b) (Olson, 1995) , and zeolite/LTW composite (black line: LTW-NaA (a), LTW-NaX (b)).

Figure 4.4 presents the XRD patterns of BW composites with zeolite NaA (BW-NaA) and zeolite NaX (BW-NaX), compared to LTW, zeolite NaA, and zeolite NaX. Similar to the trends observed in zeolite/LTW composites, BW-NaA (Figure 4.4a) exhibited characteristic peaks of zeolite NaA. However, BW-NaX (Figure 4.4b) do not display clear peaks of zeolite NaX. Compared to zeolite/LTW composites, the zeolite/BW composites showed lower peak intensity for zeolite, suggesting that LTW was better suited as a support for zeolite in the dual templating method than BW. Additionally, the peak attributed to calcite showed a weaker signal in BW-NaX than in BW-NaA, a trend similar to that observed in zeolite/LTW composites.

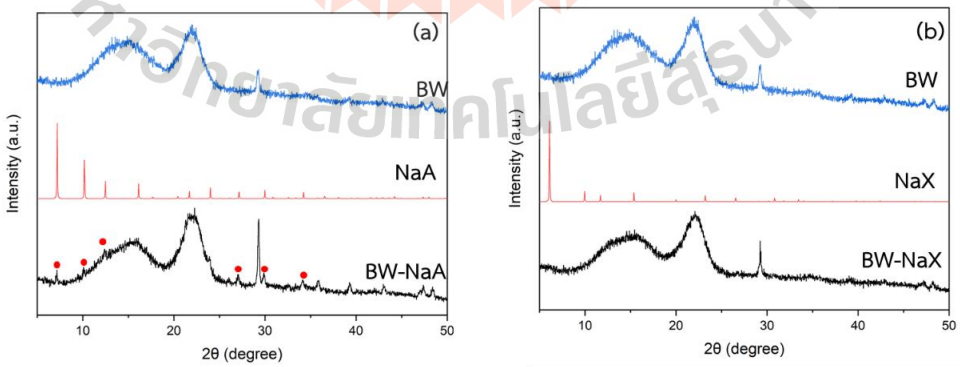

Figure 4.4 XRD pattern of BW (blue line), Zeolite (red line: NaA (a) (Pluth and Smith, 1980), NaX (b) (Olson, 1995), and zeolite/BW composite (black line: BW -NaA (a), BW -NaX (b)).

Figure 4.5 presents the SEM images of LTW composites with zeolite NaA (LTW-NaA: Figures 4.5a, 4.5b, and 4.5c) and zeolite NaX (LTW-NaX: Figures 4.5d, 4.5e, and 4.5f). In LTW-NaA, cubic crystals were observed on the LTW surface, with an average size of approximately 0.67 μm. This morphology was attributed to zeolite NaA (Khaosomboon et al., 2018). In LTW-NaX, 2.01 μm non-uniform polycrystalline structures were observed on the LTW surface, where individual crystals were held (Rongchapo et al., 2017). These findings suggested that zeolite NaX had still grown on the LTW surface but not in sufficient quantity to produce distinct zeolite peaks in the XRD analysis. In contrast, zeolite NaA exhibited a higher presence on the LTW surface, as evident in the SEM images.

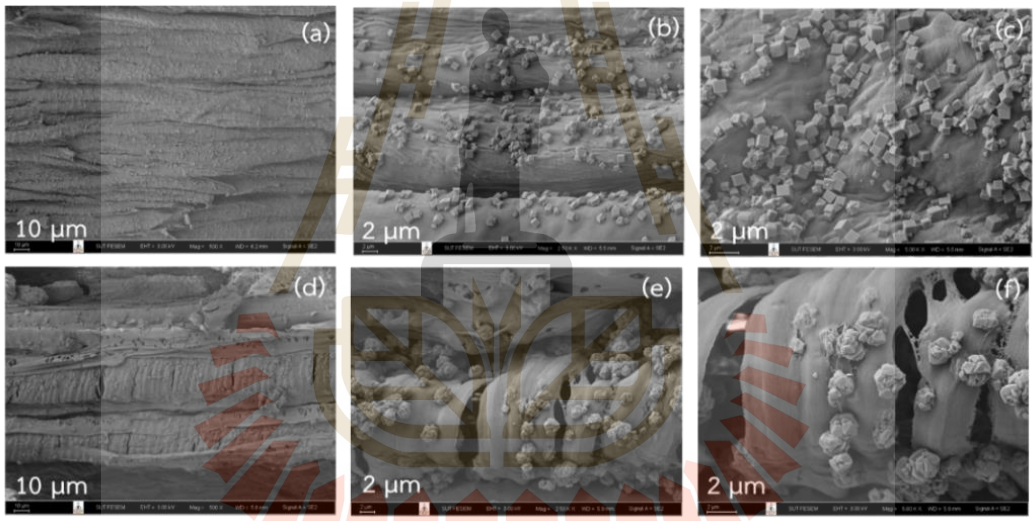

Figure 4.5 SEM images with different magnifications of zeolite/LTW composites NaA (a) 500x (b) 2500x (c) 5000x and NaX (d) 500x (e) 2500x (f) 5000x.

Figure 4.6 presents the SEM images of BW composites with zeolite NaA (BW-NaA: Figures 4.6a, 4.6b, and 4.6c) and zeolite NaX (BW-NaX: Figures 4.6d, 4.6e, and 4.6f). Both BW-NaA and BW-NaX exhibited crystals on the BW surface, displaying their respective zeolite morphologies. The crystal size in BW-NaA was approximately 1.06 μm, while in BW-NaX, it was around 1.63 μm. Compared to LTW/zeolite composites, BW/zeolite composites showed a lower quantity of zeolite on the surface. This observation was further supported by the XRD analysis, which revealed weaker zeolite signals in BW/zeolite composites than in LTW/zeolite composites.

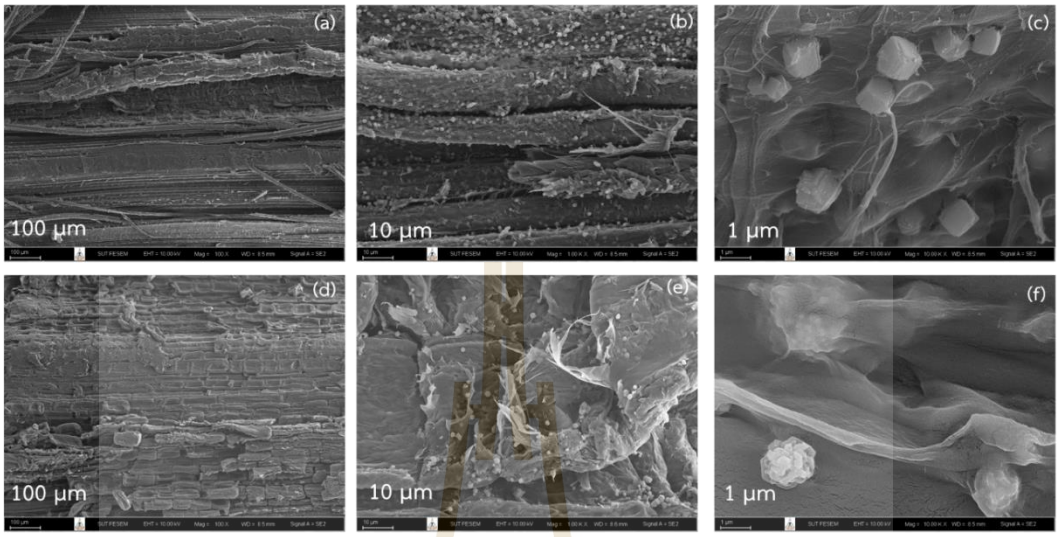

Figure 4.6 SEM images with different magnifications of zeolite/BW composites NaA (a) 500x (b) 2500x (c) 5000x and NaX (d) 500x (e) 2500x (f) 5000x.

4.1.3 Zeolite powder outside the wood

In addition to the wood samples, zeolite powders outside the wood composites were also analyzed. These powders were characterized by XRD and SEM. Figure 4.7a shows the XRD patterns of LTW-NaA-P and BW-NaA-P, which displayed only the characteristic peaks of zeolite NaA. Similarly, Figure 4.7b shows the XRD patterns of LTW-NaX-P and BW-NaX-P, which exhibited only the characteristic peaks of zeolite NaX. These results indicated that the powders collected from outside the lead tree wood and bamboo chopstick composites were pure zeolite.

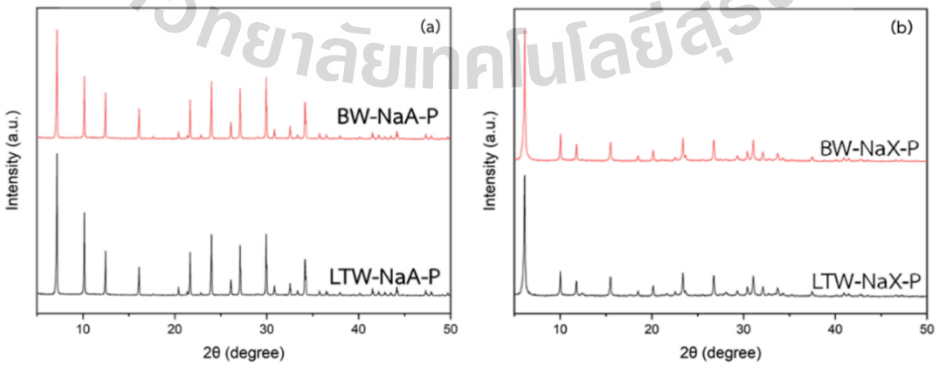

Figure 4.7 XRD pattern of zeolite NaA (4.7a) and NaX (4.7b) powder samples outside the wood.

Figure 4.8 shows the SEM images of LTW-NaA-P and LTW-NaX-P. Both zeolite samples exhibited morphologies characteristic of their respective zeolites—cubic crystals for zeolite NaA and non-uniform polycrystalline structures for zeolite NaX. However, when compared to the zeolite formed inside the wood, the zeolite NaA from outside the wood displayed a slightly different shape. The cubic crystals of NaA outside the wood appeared more rounded, whereas the crystals formed inside the wood had sharper edges. In terms of particle size, the zeolite NaA inside the wood showed a more uniform size, averaging around 0.67 μm, while the NaA crystals outside the wood ranged from 0.16 to 1.05 μm. These differences in morphology and size are likely due to the distinct crystallization environments. Inside the wood, the confined porous structure provides limited nucleation sites that promote slower, more uniform crystal growth, resulting in well-defined cubic crystals. In contrast, the bulk gel outside the wood allows rapid and less controlled crystallization, leading to more irregular, non-uniform crystals.

For zeolite NaX, the powder from outside the wood consisted of smaller individual crystals that formed the larger polycrystalline structures. These crystals were smaller than those observed inside the wood. However, overall, the zeolite NaX crystals from both inside and outside the wood exhibited similar size. The smaller crystal size observed in the zeolite formed outside the wood may be attributed to a higher nucleation density in the bulk gel compared with the more restricted nucleation environment on the wood surface.

Figure 4.9 shows the SEM images of BW-NaA-P and BW-NaX-P. Similar to the powder sample out side the lead tree wood the BW-NaA-P and BW-NaX-P show the same characteristic morphology of the NaA and NaX zeolite to the powder sample out side the lead tree wood. In terms of particle size, the zeolite NaA outside the wood showed a more uniform size, averaging around 1.57 μm, while the NaA crystals outside the wood ranged from 0.17 to 1.28 μm.

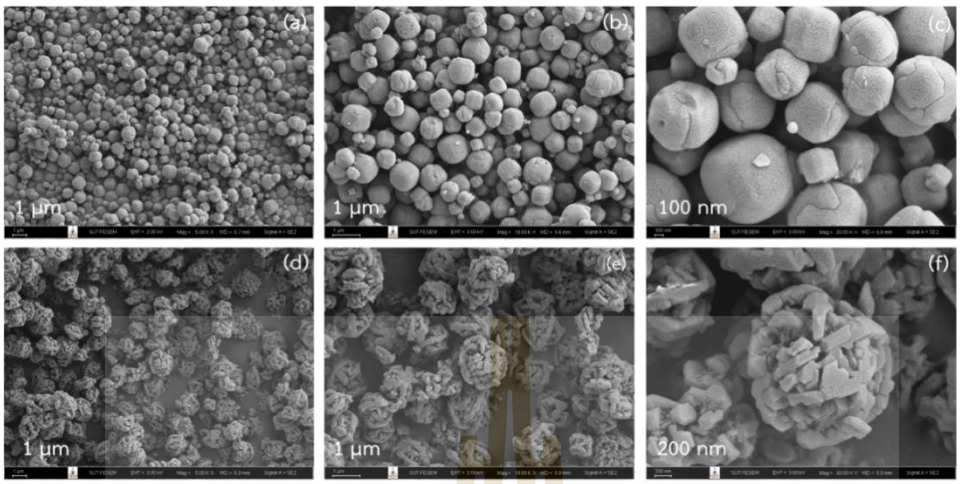

Figure 4.8 SEM images of zeolite powder samples outside the lead tree wood of zeolite NaA (a) 5000x (b) 10000x (c) 30000x and NaX (d) 5000x (e) 10000x (f) 30000x.

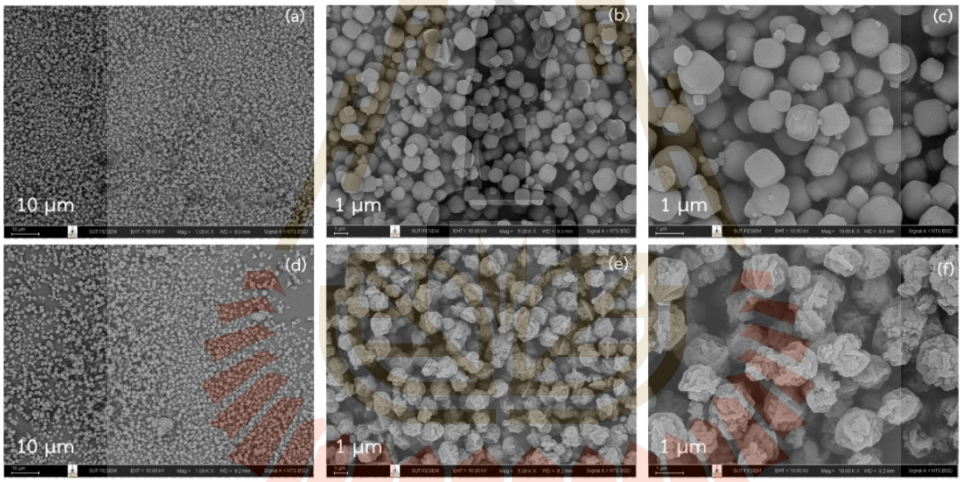

Figure 4.9 SEM images of zeolite powder samples outside the bamboo chopstick of zeolite NaX (a) 1000x (b) 5000x (c) 10000x and NaX (d) 1000x (e) 5000x (f) 10000x.

4.1.4 Thermal stability and %zeolite by TGA of wood composites

Figures 4.10 and 4.11 present the TGA (a) and DTG (b) curves of the LTW and BW samples, respectively. In all samples, the weight loss observed between 75–250°C was attributed to the evaporation of water, while the weight loss between 250–330°C corresponded to the decomposition of hemicellulose. The third stage of weight loss, occurring between 350–450°C, was associated with cellulose degradation, and the final weight loss above 450°C was due to lignin decomposition (Li et al., 2011). The remaining residue was likely to be zeolite.

The residual zeolite content indicated that the LTW samples contained a higher amount of zeolite than the BW samples, with LTW-NaA at 10.00% and LTW-NaX at 2.24%. The BW samples contained the least amount of zeolite, with BW-NaA at 4.49%, while BW-NaX was not detected by TGA analysis—likely due to its very low zeolite NaX content. This result is consistent with previous studies using zeolite NaY in non-reflux wood composites, where zeolite content was found to be 22.4% in Lead tree wood (Krukkratoke et al., 2022) and 5.46% in bamboo (Tawachkultanadilok et al., 2023).

The TGA results also indicate that zeolite NaA composites contain a higher amount of zeolite than NaX composites, likely due to differences in crystallization time. Zeolite NaA requires a shorter crystallization time (2.5 hours) compared to NaX (18 hours), suggesting that NaA forms more readily and with a higher crystallization rate than NaX. Based on the TGA results, the LTW and BW samples contain relatively low zeolite content and are therefore likely not suitable for applications such as CO_2 adsorption.

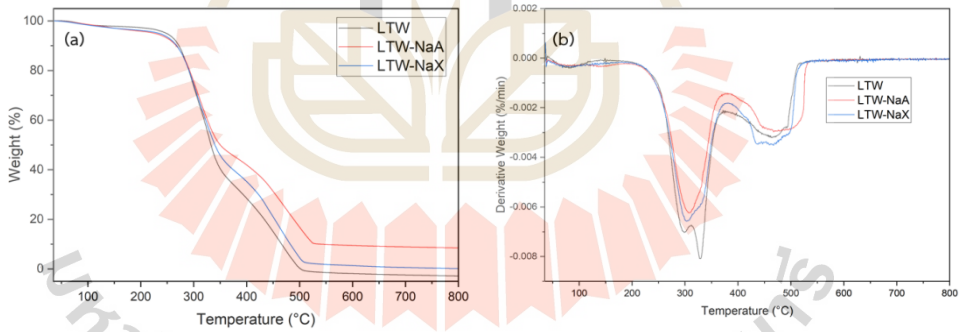

Figure 4.10 (a) TGA and (b) DTG curves of LTW samples

.

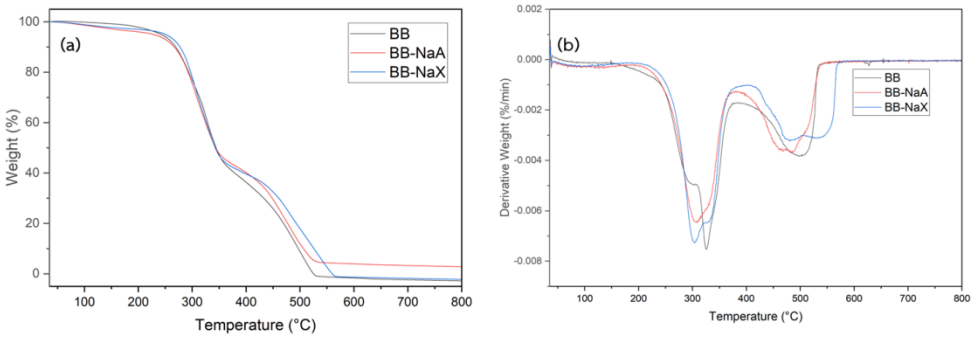

Figure 4.11 (a) TGA and (b) DTG curves of BW samples.

4.2 Characterization of paper composites

4.2.1 XRD pattern and SEM images of paper composites

Since LTW and BW are not suitable for CO_2 adsorption, a different type of material with potentially higher zeolite content was synthesized—paper made from sugarcane leaves (SLP), combined with zeolite NaA and zeolite NaX (referred to as SLP-NaA and SLP-NaX, respectively). These materials can be used in fruit packaging to adsorb gases released by fruit, such as CO_2, to prevent damage to fruit tissue (Krupa and Tomala, 2021) and ethylene, to slow the ripening process (do Nascimento Sousa et al., 2020). The SLP samples were analyzed using XRD, SEM, and TGA.

Figure 4.12 presents the XRD pattern of SLP. Compared to the XRD patterns of LTW and BW, SLP exhibited similar peak positions; however, the two broad peaks at 14° and 22° had lower intensity. Additionally, SLP do not show clear calcite patterns, except for a sharp peak at 29°, which appears with a weaker signal. This was likely due to the NaOH treatment used during the pulp-making process.

Figure 4.13 shows the morphology of SLP. Figure 4.13a shows the overall structure of SLP that is made of many fibers (Figure 4.13b) connected by some materials (Figure 4.13c), which may be lignin or extractives. (Wutisatwongkul et al., 2016) .SEM images revealed that these materials had rough surfaces.

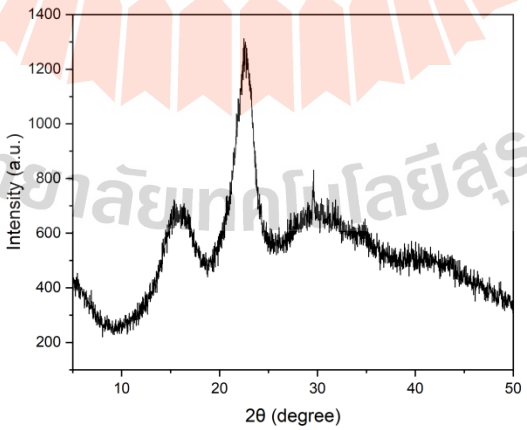

Figure 4.12 XRD pattern of SLP.

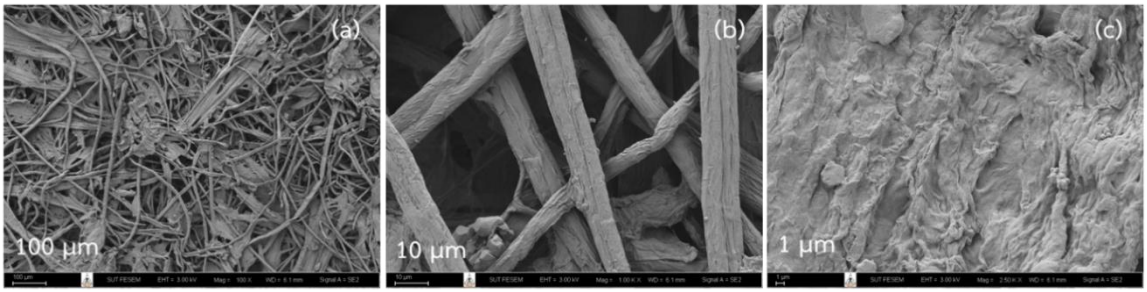

Figure 4.13 SEM images with different magnifications of SLP (a) 100x (b) 1000x (c) 2500x

4.2.2 XRD pattern and SEM images of zeolite composites with paper

Figure 4.14 presents the XRD patterns of SLP composites with zeolite NaA (SLP-NaA) and zeolite NaX (SLP-NaX), compared to SLP, zeolite NaA, and zeolite NaX. The XRD patterns of both SLP-NaA and SLP-NaX exhibit characteristic peaks corresponding to their respective zeolite counterparts. However, compared to LTW/zeolite and BW/zeolite composites, the XRD patterns of SLP/zeolite composites appear much clearer. This indicated that the synthesis method used for SLP composites resulted in a higher zeolite content than the dual templating method.

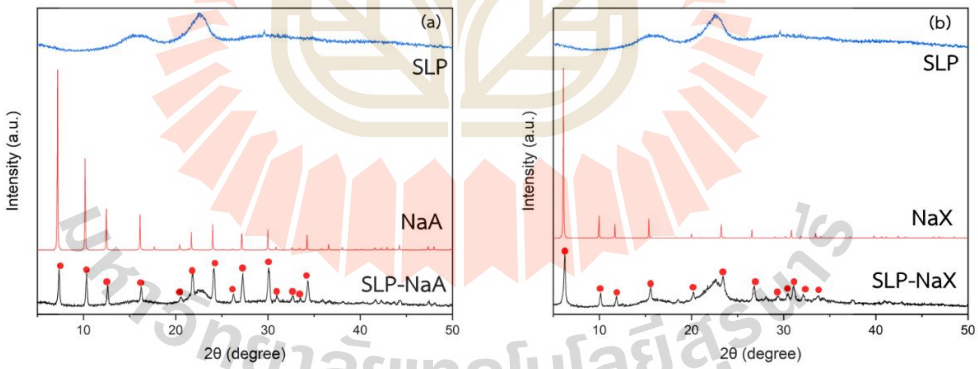

Figure 4.14 XRD pattern of SLP (blue line), Zeolite (red line: NaA (a) (Pluth and Smith, 1980), NaX (b) (Olson, 1995) , and zeolite/SLP composite (black line: BW -NaA (a), BW -NaX (b)).

Figure 4.15 presents the SEM images of SLP composites with zeolite NaA (SLP-NaA: Figures 4.15a, 4.15b, and 4.15c) and zeolite NaX (SLP-NaX: Figures 4.15d, 4.15e, and 4.15f). SLP-NaA exhibited crystals with the characteristic morphology of zeolite NaA, measuring approximately 0.35-0.92 μm, while SLP-NaX displayed crystals resembling zeolite NaX, with a size of around 1.53 μm. In terms of zeolite quantity, SLP/zeolite composites contained significantly more zeolite than both LTW/zeolite and BW/zeolite composites.

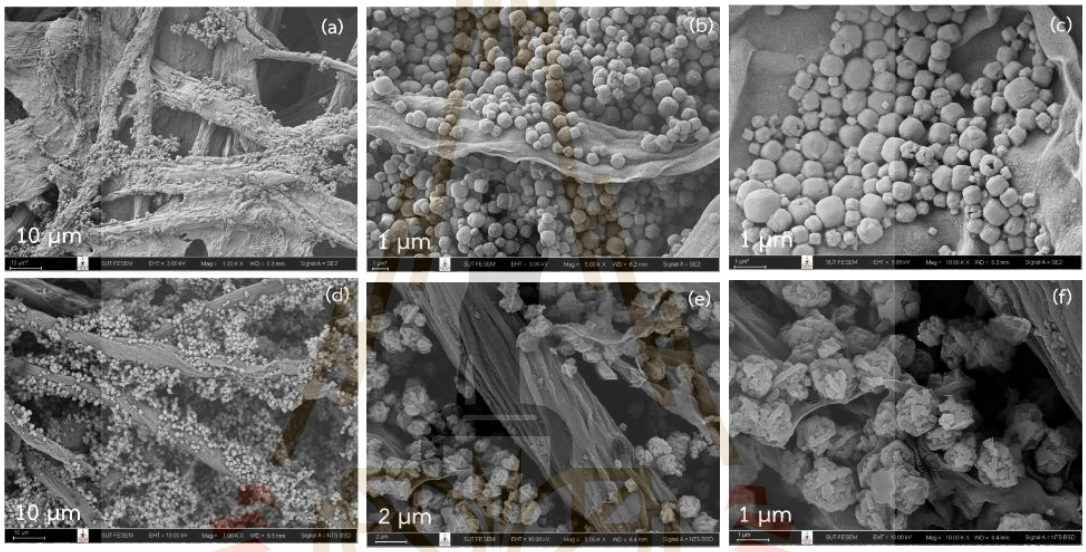

Figure 4.15 SEM images with different magnifications of zeolite/SLP composites NaA (a) 1000x (b) 5000x (c) 10000x and NaX (d) 1000x (e) 5000x (f) 10000x.

4.2.3 Zeolite powder before adding into paper pulp

In addition to the paper samples, the zeolite powders before being added to the paper pulp were also analyzed. These powders were characterized by XRD and SEM. Figures 4.16a and 4.16b show the synthesized zeolite NaA and NaX powders, respectively, before their addition to the paper pulp. The XRD patterns displayed characteristic peaks corresponding to their respective zeolites, confirming that the powders were pure zeolite.

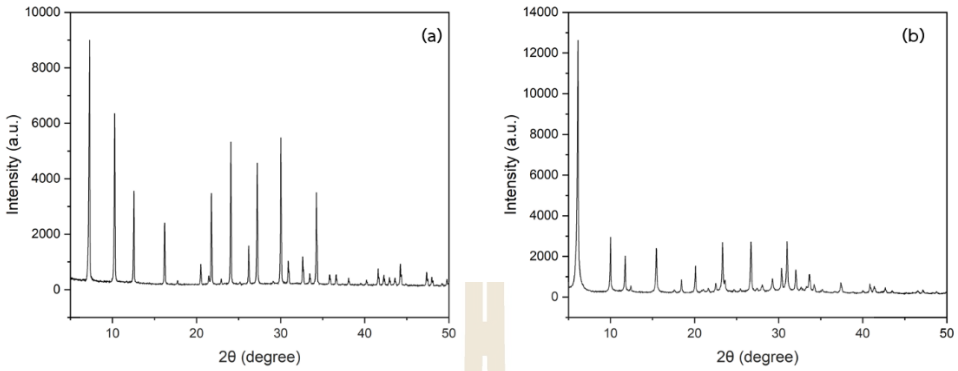

Figure 4.16 XRD pattern of zeolite NaA (4.15a) and NaX (4.15b) powder before adding into paper pulp

Figure 4.17 presents the SEM images of the zeolite powders before being added to the paper pulp. The SEM images showed that both zeolite NaA and NaX powders exhibited the same morphology as their respective zeolites in the paper composites, in terms of both shape and size. Zeolite NaA particles ranged from approximately 0.36 to 0.97 μm, while zeolite NaX particles measured around 1.33 μm.

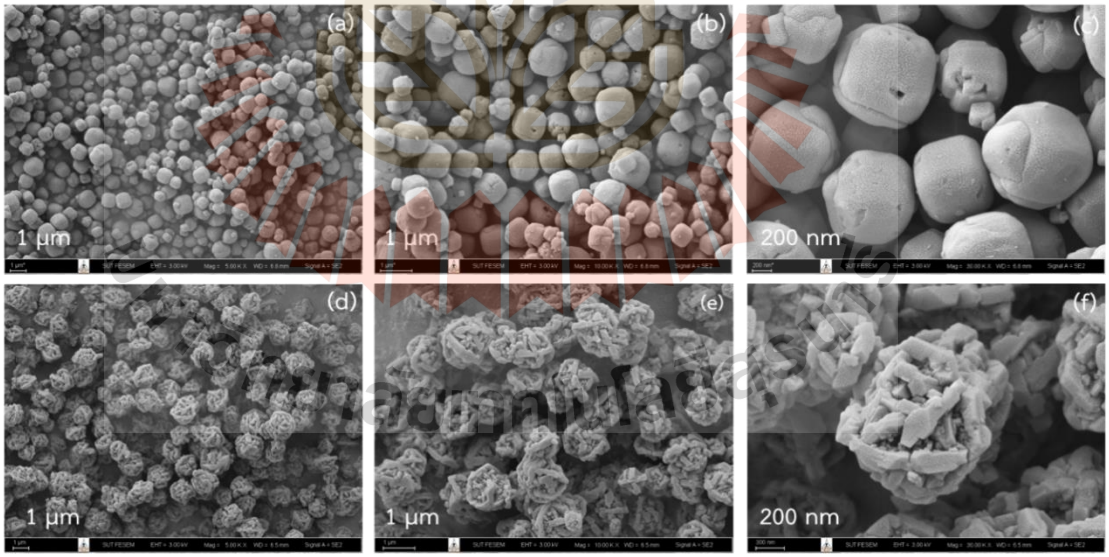

Figure 4.17 SEM images of zeolite powder samples before adding into paper pulp of NaA (a) 5000x (b) 10000x (c) 3000x and NaX (d) 5000x (e) 10000x (f) 30000x.

4.2.4 Thermal stability and %zeolite by TGA of paper composites

Figure 4.18 presents the TGA (a) and DTG (b) curves of the SLP samples. The TGA profiles show that SLP undergoes pyrolysis similar to that of the LTW and BW samples, beginning with the loss of water, followed by the decomposition of hemicellulose and lignin, respectively. The remaining residue indicates that the SLP composites contain significantly higher amounts of zeolite compared to the LTW and BW composites. The SLP composites also follow the same trend as LTW and BW, with the NaA composites (29.78%) containing more zeolite than the NaX composites (19.03%). This is likely due to the smaller particle size of zeolite NaA, which allows it to disperse more easily and embed more effectively within the pulp fibers during mixing.

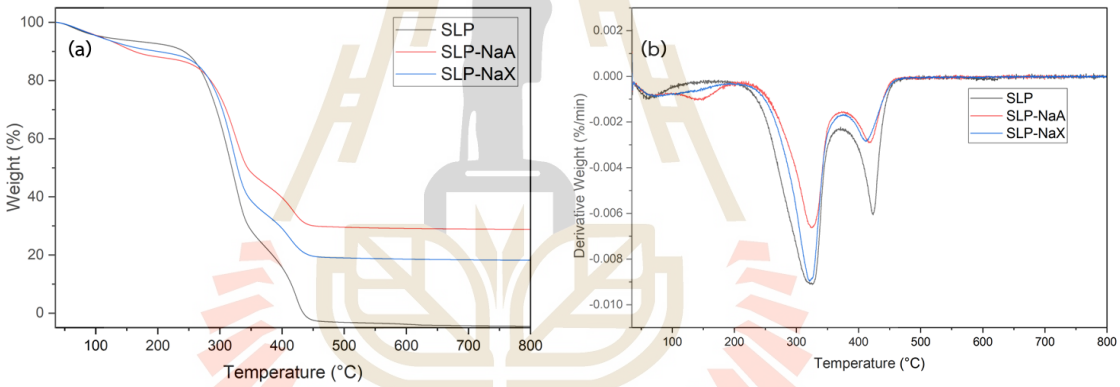

Figure 4.18 (a) TGA and (b) DTG curves of SLP samples.

4.2.5 Adsorption isotherm by N_2 adsorption of paper composites

The surface area, pore diameter, and pore volume were determined using N_2 adsorption with an Autosorb iQ instrument. These values were calculated based on the quantity of nitrogen adsorbed and desorbed by the material at a constant liquid nitrogen temperature of −196°C using the BET method. Due to the low amount of zeolite in LTW/zeolite and BW/zeolite composites, it was determined that both materials were not suitable for CO_2 adsorption. As a result, they were excluded from N_2 adsorption and CO_2 adsorption experiments. Figure 4.19 presents the N_2 adsorption–desorption isotherms of SLP, SLP-NaA, and SLP-NaX. It is worth noting that in the zeolite NaA composite, the smaller pore size (4 Å) and the positioning of Na^+ cations near the

micropore apertures prevented an accurate surface area measurement using nitrogen sorption (Madhu et al., 2022).

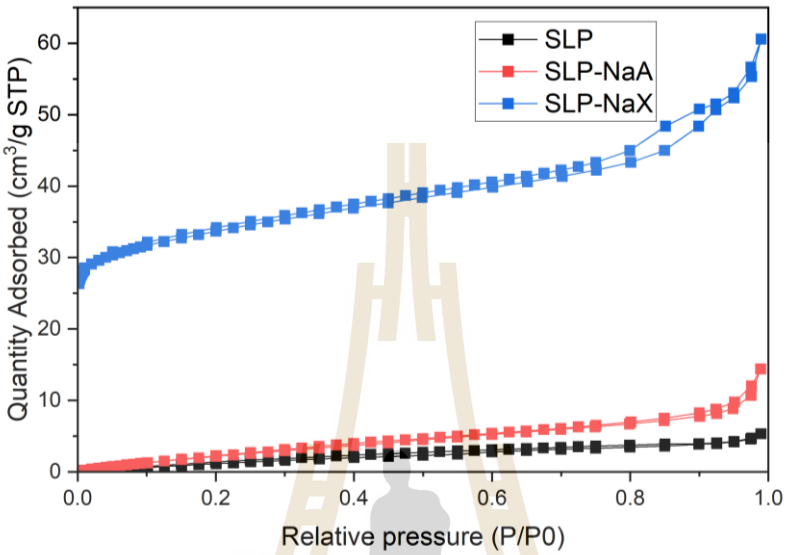

Figure 4.19 Isotherm of SLP materials.

Figure 4.19 also shows that all materials exhibited nitrogen adsorption, with SLP-NaA displaying relatively low adsorption due to the limitations of zeolite NaA. However, SLP-NaA still demonstrated increased N_2 adsorption compared to SLP. According to IUPAC classification, both SLP and SLP-NaA exhibited a type II isotherm, indicating their non-porous or macroporous structure (Kajama et al., 2015). SLP-NaX showed the highest nitrogen adsorption volume due to its larger pore size, despite containing a lower amount of zeolite than SLP-NaA. The type I isotherm classification indicated that SLP-NaX had a microporous structure (Schlumberger and Thommes, 2021). Additionally, all materials exhibited a hysteresis loop, confirming the presence of mesopores (Schlumberger and Thommes, 2021).

Table 4.1 presents the N_2 adsorption isotherm properties of SLP materials. Pore size distribution was obtained using the Barrett–Joyner–Halenda (BJH) equation. For SLP-NaA, the introduction of zeolite NaA into SLP resulted in a slight increase in BET surface area from 8 m^2/g to 13 m^2/g, attributed to the pore limitations of zeolite NaA. In contrast, SLP-NaX exhibited a significant increase in nitrogen adsorption, with a BET

surface area of 126 m²/g. This increase was due to the larger pore diameter of zeolite NaX, making it more suitable for nitrogen adsorption.

Table 4.1 Surface area, pore volume and diameter of SLP materials.

Sample	S_{BET} (m^2/g)	Pore Volume (cm^3/g)	Pore Diameter (nm)
SLP	8	0.01	3.3
SLP-NaA	13	0.02	3.1
SLP-NaX	126	0.05	3.1

4.3 CO_2 and ethylene adsorption studies

4.3.1 CO_2 adsorption studies

The CO_2 adsorption isotherm was obtained using a BELSORP MAX X instrument at a 298.15 K, with the pressure range 0–100 kPa. Figure 4.20 presented the CO_2 adsorption isotherm of SLP samples. The results showed that SLP-NaA exhibited the highest CO_2 adsorption capacity, surpassing that of SLP-NaX, despite zeolite NaX having a larger pore diameter than zeolite NaA. Typically, zeolite NaX would be expected to adsorb more CO_2 than zeolite NaA (Boer et al., 2023); however, this discrepancy was likely due to the higher zeolite content in SLP-NaA compared to SLP-NaX. When compared to N_2 adsorption, SLP-NaA demonstrated superior performance in CO_2 adsorption. This was attributed to the stronger interaction between zeolite and CO_2 compared to N_2, given that CO_2 has a lower kinetic diameter (3.30 Å to 3.64 Å), a higher quadrupole moment (13.4×10^{-40} C/m² to 4.6×10^{-40} C/m²), and greater polarizability (2.65×10^{-24} cm³ to 1.76×10^{-24} cm³) (Boer et al., 2023).

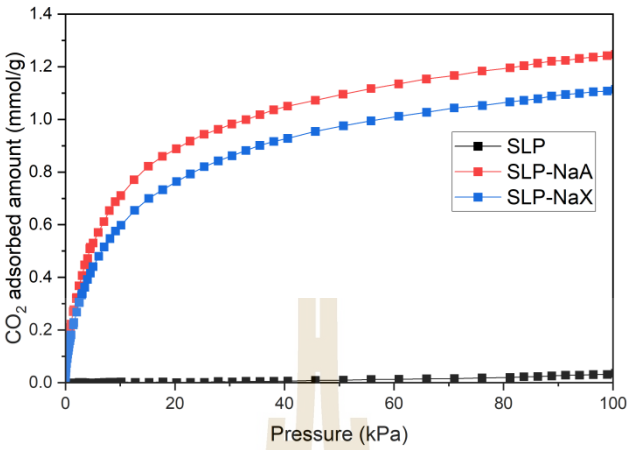

Figure 4.20 CO_2 adsorption isotherm of SLP samples.

The results showed that SLP adsorbed CO_2 only 0.036 mmol/g. The addition of zeolite significantly increased CO_2 adsorption, with SLP-NaA reaching 1.25 mmol/g and SLP-NaX reaching 1.11 mmol/g. The CO_2 adsorption data were then fitted using a non-linear curve fit with Langmuir, Freundlich, Toth, and Langmuir-Freundlich isotherm models, as shown in Figure 4.21. The corresponding parameter values are presented in Table 4.2. The results indicated that both composites followed the Langmuir-Freundlich isotherm model.

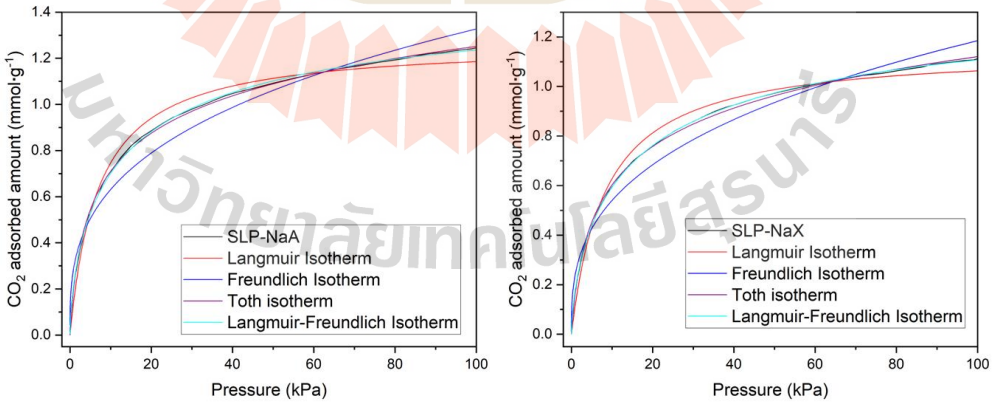

Figure 4.21 CO_2 adsorption isotherm fitting of zeolite/SLP composites.

Table 4.21 CO_2 adsorption isotherm fitting of SLP/Zeolite composites.

Samples	Correlation coefficients (R^2)			
	Langmuir isotherm	Freundlich isotherm	Toth isotherm	Langmuir-Freundlich isotherm
SLP-NaA	0.9895	0.9769	0.9986	0.9996
SLP-NaX	0.9904	0.9802	0.9988	0.9999

Due to the smaller pore size of zeolite NaA, it exhibited better selectivity than zeolite NaX (Boer et al., 2023). This result indicated that SLP-NaA was the most effective material for CO_2 adsorption, as it had the highest adsorption capacity due to its higher zeolite content. Furthermore, SLP-NaA demonstrated potential for use as a selective material for CO_2 adsorption.

4.3.2 Ethylene adsorption studies

Ethylene-TPD was used to study the adsorption of ethylene on SLP samples, compared to TPD runs without gas. Figures 4.22, 4.23, and 4.24 present the results, which showed that all samples exhibited desorption at around 200°C, which is likely due to residual adsorbed water within the cavities rather than ethylene, as the TPD without gas also showed desorption at the same temperature. Both SLP and SLP-NaX showed no ethylene-related desorption peaks other than at 200°C. In the case of SLP, this is likely because it either does not adsorb ethylene or only adsorbs a very small amount. For SLP-NaX, the lack of ethylene desorption may be due to stronger interactions between ethylene and the zeolite, requiring a higher temperature for desorption. However, temperatures above 200°C pose a risk of decomposing the composites, indicating that SLP-NaX is not suitable for ethylene adsorption due to its lack of regenerability.

In contrast, the ethylene-TPD of SLP-NaA showed a distinct desorption peak at 111.5°C, which was not present in the TPD without gas, indicating that this peak is likely due to ethylene. Integration of the area under the curve revealed that SLP-NaA desorbed ethylene in an amount of 0.034 mmol/g.

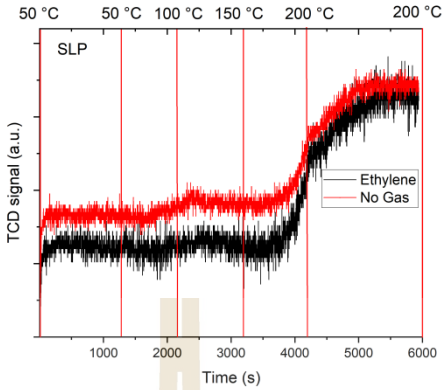

Figure 4.22 TPD profile of SLP with ethylene (black line) and without TPD (red line).

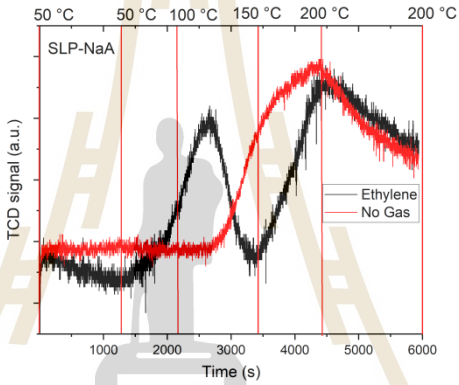

Figure 4.23 TPD profile of SLP-NaA with ethylene (black line) and without TPD (red line).

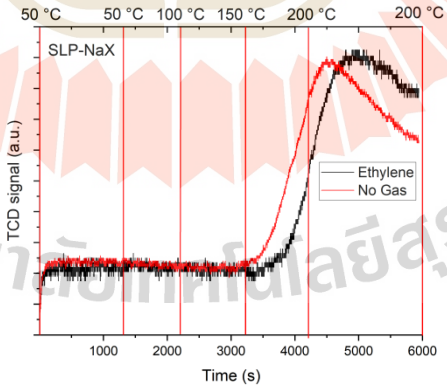

Figure 4.24 TPD profile of SLP-NaX with ethylene (black line) and without TPD (red line).

To further confirm ethylene desorption from the samples, zeolite NaA and NaX powder samples—prior to their addition to the paper pulp—were analyzed using ethylene-TPD following the method of Manadee et al. (2012). Before the analysis, the zeolites were degassed at 500°C for 1 hour under a helium atmosphere. After cooling to 50°C, ethylene diluted with inert gas (7.5% C_2H_4/He) was introduced for 30 minutes. Subsequently, the zeolites were purged with helium for 1 hour to remove physisorbed species. The temperature was then ramped from 100 to 810°C.

Figure 4.25 shows the ethylene-TPD results of the zeolite NaA and NaX powders. Zeolite NaA exhibited ethylene desorption at 111.7°C and 379.1°C, which agrees with the desorption peak observed in the SLP-NaA sample at 111.5°C—further confirming that the signal at 111.5°C corresponded to ethylene desorption. In contrast, zeolite NaX showed ethylene desorption only at 335.4°C, confirming that the SLP-NaX sample did not desorb ethylene below 200°C. These results demonstrated that only SLP-NaA was suitable for ethylene adsorption.

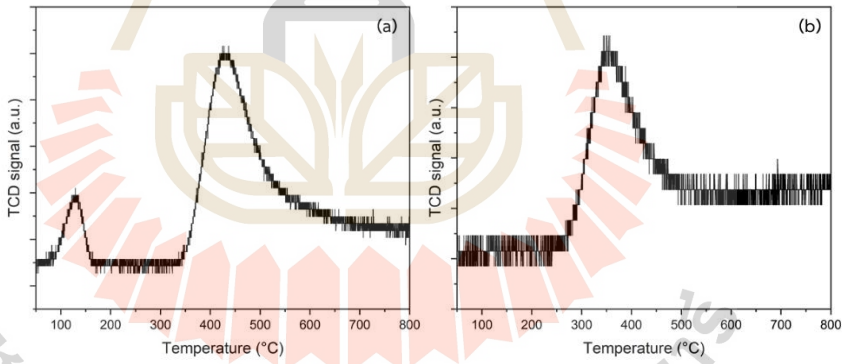

Figure 4.25 Ethylene-TPD profile of zeolite powder samples before adding into paper pulp of zeolite NaA (a) and zeolite NaX (b).

CHAPTER V
CONCLUSIONS

Zeolite NaA and NaX in Lead tree wood and bamboo chopstick composites were synthesized using hydrothermal methods. The overall gel composition for zeolite NaA followed a molar ratio of $6Na_2O:Al_2O_3:SiO_2:150H_2O$, while that for zeolite NaX was $NaAlO_2:4SiO_2:16NaOH:88H_2O$. The XRD patterns of both non-composite Lead tree wood and bamboo chopsticks showed characteristic cellulose peaks along with calcite impurities. SEM images revealed the presence of zeolite crystals with morphology typical of their respective types—cubic for NaA and irregular polycrystalline for NaX. TGA results showed that LTW composites contained more zeolite than BW composites, with NaA composites exhibiting higher zeolite content than NaX. However, both types of wood-based composites had low overall zeolite content and were not suitable for CO_2 adsorption applications.

To address the limitation of low zeolite content in wood composites, paper composites made from sugarcane leaves with embedded zeolite were synthesized as an alternative. The XRD patterns of the SLP composites displayed similar features to those of LTW and BW, but with reduced calcite impurities. SEM images showed comparable zeolite morphologies but with a higher density of zeolite crystals in the paper matrix. TGA analysis confirmed that SLP composites contained significantly more zeolite than wood composites—29.78% for NaA and 19.03% for NaX. Nitrogen adsorption studies revealed that the paper composite with zeolite NaX exhibited the highest nitrogen uptake, resulting in the largest BET surface area (126 m^2/g), despite its lower zeolite content. In contrast, the paper composite with zeolite NaA adsorbed only a small amount of nitrogen due to the smaller pore size of NaA, leading to a modest increase in surface area compared to paper without zeolite (from 8 m^2/g to 13 m^2/g). The isotherm type observed for NaA was type II, whereas NaX showed a type I isotherm, indicative of microporous structures.

The CO_2 adsorption study revealed a different trend compared to nitrogen adsorption. In this case, the paper composite with zeolite NaA exhibited the highest CO_2 adsorption capacity (1.25 mmol/g), surpassing that of the NaX composite (1.11 mmol/g). This was attributed to the stronger interaction between CO_2 and the zeolite framework, as well as the higher zeolite content in the NaA composite. Isotherm model fitting indicated that the paper/zeolite composites followed the Langmuir–Freundlich isotherm model. Ethylene adsorption, evaluated by temperature-programmed desorption (TPD), showed that only the paper composite with zeolite NaA was suitable for ethylene adsorption. The NaX composite was not suitable due to its lack of regenerability, as desorption required

REFERENCES

REFERENCES

Adeoye, M. D., Lawal, A. T., Jimoh, A. O., Adelani, A. K., Ojo, O. O., Ndukwe, N. A., Salaudeen, T., and Adewuyi, S. (2021). Fascinating physical-chemical properties and fiber morphology of selected waste plant leaves as potential pulp and paper making agents. *Biomass Conversion and Biorefinery, 11*(6), 3061-3070. doi:10.1007/s13399-020-00968-8

Álvarez-Hernández, M. H., Artés-Hernández, F., Ávalos-Belmontes, F., Castillo-Campohermoso, M. A., Contreras-Esquivel, J. C., Ventura-Sobrevilla, J. M., and Martínez-Hernández, G. B. (2018). Current scenario of adsorbent materials used in ethylene scavenging systems to extend fruit and vegetable postharvest life. *Food and Bioprocess Technology, 11*(3), 511-525. doi:10.1007/s11947-018-2076-7

Boer, D. G., Langerak, J., and Pescarmona, P. P. (2023). Zeolites as selective adsorbents for CO_2 separation. *ACS Applied Energy Materials, 6*(5), 2634-2656. doi:10.1021/acsaem.2c03605

Cherian, S., Figueroa, C. R., and Nair, H. (2014). 'Movers and shakers' in the regulation of fruit ripening: a cross-dissection of climacteric versus non-climacteric fruit. *Journal of Experimental Botany, 65*(17), 4705-4722. doi:10.1093/jxb/eru280

Choi, S., Drese, J. H., and Jones, C. W. (2009). Adsorbent materials for carbon dioxide capture from large anthropogenic point sources. *ChemSusChem, 2*(9), 796-854. doi:10.1002/cssc.200900036

Chokwarakul, K. (2018). The efficient development and productivity to raise the value added of the manufacturing industry, agriculture, "Cane" in the Northeast. *Research Community and Social Development Journal, 12*(1), 181-190.

Costa, E., Calleja, G., Jimenez, A., and Pau, J. (1991). Adsorption equilibrium of ethylene, propane, propylene, carbon dioxide, and their mixtures on 13X zeolite. *Journal of Chemical & Engineering Data, 36*(2), 218-224. doi:10.1021/je00002a020

Couck, S., Lefevere, J., Mullens, S., Protasova, L., Meynen, V., Desmet, G., Baron, G. V., and Denayer, J. F. M. (2017). CO_2, CH_4 and N_2 separation with a 3DFD-printed ZSM-5 monolith. *Chemical Engineering Journal, 308*, 719-726. doi:10.1016/j.cej.2016.09.046

Dabbawala, A. A., Ismail, I., Vaithilingam, B. V., Polychronopoulou, K., Singaravel, G., Morin, S., Berthod, M., and Al Wahedi, Y. (2020). Synthesis of hierarchical porous Zeolite-Y for enhanced CO_2 capture. *Microporous and Mesoporous Materials, 303*, 110261. doi:10.1016/j.micromeso.2020.110261

Dhall, R. (2013). Ethylene in Post-harvest Quality Management of Horticultural Crops: A Review. *Research & Reviews: A Journal of Crop Science and Technology, 2*, 9-25.

do Nascimento Sousa, S. D., Santiago, R. G., Soares Maia, D. A., de Oliveira Silva, E., Vieira, R. S., and Bastos-Neto, M. (2020). Ethylene adsorption on chitosan/zeolite composite films for packaging applications. *Food Packaging and Shelf Life, 26*, 100584. doi:10.1016/j.fpsl.2020.100584

Domínguez, I., Lafuente, M. T., Hernández-Muñoz, P., and Gavara, R. (2016). Influence of modified atmosphere and ethylene levels on quality attributes of fresh tomatoes (Lycopersicon esculentum Mill.). *Food Chemistry, 209*, 211-219. doi:10.1016/j.foodchem.2016.04.049

Du, X. (2013). Molecular-dynamics simulation of self-diffusion of molecular hydrogen in X-type zeolite. *Journal of Chemistry, 2013*(1), 545367. doi: 10.1155/2013/545367

Gan, F., Wang, B., Jin, Z., Xie, L., Dai, Z., Zhou, T., and Jiang, X. (2021). From typical silicon-rich biomass to porous carbon-zeolite composite: A sustainable approach for efficient adsorption of CO_2. *Science of The Total Environment, 768*, 144529. doi:10.1016/j.scitotenv.2020.144529

Gautam, Serafin, J., Vikram, S., Dziejarski, B., and Sahoo, S. (2023). An environmentally friendly synthesis method of activated carbons based on subabul (Leucaena leucocephala) sawdust waste for CO_2 adsorption. *Journal of Cleaner Production, 412*, 137406. doi:10.1016/j.jclepro.2023.137406

Georgieva, V. M., Bruce, E. L., Verbraeken, M. C., Scott, A. R., Casteel, W. J., Jr., Brandani, S., and Wright, P. A. (2019). Triggered gate opening and breathing effects during selective CO_2 adsorption by merlinoite zeolite. *Journal of the American Chemical Society, 141*(32), 12744-12759. doi:10.1021/jacs.9b05539

Guan, R., Su, J., Meng, X., Li, S., Liu, Y., Xu, J., and Zhang, S. (2015). Multilayered regulation of ethylene induction plays a positive role in arabidopsis resistance against pseudomonas syringae *Plant Physiology, 169*(1), 299-312. doi:10.1104/pp.15.00659

Guo, Y., Sun, T., Gu, Y., Liu, X., Ke, Q., Wei, X., and Wang, S. (2018). Rational Synthesis of Chabazite (CHA) Zeolites with Controlled Si/Al Ratio and Their $CO_2/CH_4/N_2$ Adsorptive Separation Performances. *Chemistry – An Asian Journal, 13*(21), 3222-3230. doi:10.1002/asia.201800930

Hazim, M., Mohamad Amini, M. H., Mat Rasat, M. S., Rasat, M., Ahmad, I., Wahab, R., Elham, P., Mohd, W., Wan, N., Rahman, A., Ramle, N., Kelantan, M., Jeli, Pahang, M., Jengka, B., and Pahang, M. (2017). Chemical composition of small diameter wild leucaena leucocephala species. *ARPN Journal of Engineering and Applied Sciences, 12*, 3196-3173.

Hyun, S. H., and Danner, R. P. (1982). Equilibrium adsorption of ethane, ethylene, isobutane, carbon dioxide, and their binary mixtures on 13X molecular sieves. *Journal of Chemical & Engineering Data, 27*(2), 196-200. doi:10.1021/je00028a029

Iftitahiyah, V., Prasetyoko, D., Nur, H., Bahruji, H., and Hartati, H. (2018). Synthesis and characterization of zeolite NaX from Bangka Belitung Kaolin as alternative precursor. *Malaysian Journal of Fundamental and Applied Sciences, 14*, 414-418. doi:10.11113/mjfas.v14n4.964

Izadyar, S., and Fatemi, S. (2013). Fabrication of X Zeolite Based Modified Nano TiO2 Photocatalytic Paper for Removal of VOC Pollutants under Visible Light. *Industrial & Engineering Chemistry Research, 52*(32), 10961-10968. doi:10.1021/ie400416e

Jantarit, N., Tayraukham, P., Osakoo, N., Föttinger, K., and Wittayakun, J. (2020). Formation of EMT/FAU intergrowth and nanosized SOD zeolites from synthesis gel of zeolite NaX containing ethanol. *Materials Research Express, 7*. doi:10.1088/2053-1591/aba55a

Jodnok, S., Choeisai, P., Kruehong, C., and Choeisai, K. (2021). Recycling disposable bamboo chopstick waste as a renewable energy resource: Case study in Khon Kaen University, Thailand. *Sustainable Environment Research, 31*(1), 30. doi:10.1186/s42834-021-00101-y

Kajama, M. N., Nwogu, N. C., and Gobina, E. (2015). Hydrogen permeation using nanostructured silica membranes. *WIT Transactions on Ecology and the Environment, 193*, 447-456. doi:10.2495/SDP150381

Kawon, K., Sarawong, S., and Wilaikaew, A. (2022). Value of Willingness to Accept the Difference in Purchase Price of Green Sugarcane and Burned Sugarcane of Farmers in Pak Puan Sub-District, Wang Saphung District, Loei Province. *LRUJ, 17*(61), 17-25.

Kazan, K. (2015). Diverse roles of jasmonates and ethylene in abiotic stress tolerance. *Trends in Plant Science, 20*(4), 219-229. doi:10.1016/j.tplants.2015.02.001

Keawkumay, C., Krukkratoke, P., Youngjan, S., Osakoo, N., Deekamwong, K., Khemthong, P., Phanthasri, J., Prayoonpokarach, S., and Wittayakun, J. (2024). Extraction of silica from sugarcane bagasse ash and its utilization in zeolite 4A synthesis for CO_2 adsorption. *RSC Advances, 14*(27), 19472-19482. doi:10.1039/D4RA02207F

Keawkumay, C., Sosa, N., Osakoo, N., Prayoonpokarach, S., Wittayakun, J., Youngjan, S., Boonyoung, P., Khemthong, P., Amedlous, A., and Mintova, S. (2025). Effect of aluminum source and water content in the precursor suspensions used for the synthesis of nanosized zeolite Y on CO_2 adsorption capacity. *Microporous and Mesoporous Materials, 386*, 113491. doi:10.1016/j.micromeso.2025.113491

Keller, N., Ducamp, M.-N., Robert, D., and Keller, V. (2013). Ethylene Removal and Fresh Product Storage: A Challenge at the Frontiers of Chemistry. Toward an Approach by Photocatalytic Oxidation. *Chemical Reviews, 113*(7), 5029-5070. doi:10.1021/cr900398v

Khaosomboon, P., Khuanmar, K., and Weerayutsil, P. (2018). Synthesis of zeolite-A and zeolite-Y using silica gel waste as silica source and modifying with Fe. *International Journal of Engineering & Technology, 7*, 1376. doi:10.14419/ijet.v7i4.38.27878

Koo-amornpattana, W., Jonglertjunya, W., Phadungbut, P., Ratchahat, S., Kunthakudee, N., Chalermsinsuwan, B., and Hunsom, M. (2022). Valorization of spent disposable wooden chopstick as the CO_2 adsorbent for a CO_2/H_2 mixed gas purification. *Scientific Reports, 12*(1), 11364. doi:10.1038/s41598-022-15531-w

Krishnamurthy, M., Msm, K., and Kanakkampalayam Krishnan, C. (2016). Hierarchically structured MFI zeolite monolith prepared using agricultural waste as solid template. *Microporous and Mesoporous Materials, 221*, 23-31. doi:10.1016/j.micromeso.2015.09.022

Krukkratoke, P., Keawkumay, C., Tayraukham, P., Prompiputtanapon, K., Khemthong, P., Prayoonpokarach, S., and Wittayakun, J. (2022). Strategic Synthesis to Disperse Zeolite NaY in Lead Tree Wood. *Crystals, 12*(4). doi:10.3390/cryst12040504

Krupa, T., and Tomala, K. (2021). Effect of Oxygen and Carbon Dioxide Concentration on the Quality of Minikiwi Fruits after Storage. *Agronomy, 11*(11), 2251. Retrieved from https://www.mdpi.com/2073-4395/11/11/2251

Lee, C. L., Chin, K. L., H'ng, P. S., Hafizuddin, M. S., and Khoo, P. S. (2022). Valorisation of Underutilized Grass Fibre (Stem) as a Potential Material for Paper Production. *Polymers, 14*(23), 5203. Retrieved from https://www.mdpi.com/2073-4360/14/23/5203

Li, J., Lu, Y., Yang, D., Sun, Q., Liu, Y., and Zhao, H. (2011). Lignocellulose Aerogel from Wood-Ionic Liquid Solution (1-Allyl-3-methylimidazolium Chloride) under Freezing and Thawing Conditions. *Biomacromolecules, 12*(5), 1860-1867. doi:10.1021/bm200205z

Liu, Q., Mace, A., Bacsik, Z., Sun, J., Laaksonen, A., and Hedin, N. (2010). NaKA Sorbents With High CO_2-Over-N_2 Selectivity and High Capacity to Adsorb CO_2. *Chemical Communications, 46*(25), 4502-4504. doi:10.1039/C000900H

Loiola, A. R., Andrade, J. C. R. A., Sasaki, J. M., and da Silva, L. R. D. (2012). Structural analysis of zeolite NaA synthesized by a cost-effective hydrothermal method using kaolin and its use as water softener. *Journal of Colloid and Interface Science, 367*(1), 34-39. doi:10.1016/j.jcis.2010.11.026

Lozinska, M. M., Mowat, J. P. S., Wright, P. A., Thompson, S. P., Jorda, J. L., Palomino, M., Valencia, S., and Rey, F. (2014). Cation Gating and Relocation during the Highly Selective "Trapdoor" Adsorption of CO_2 on Univalent Cation Forms of Zeolite Rho. *Chemistry of Materials, 26*(6), 2052-2061. doi:10.1021/cm404028f

Madhu, J., Santhanam, A., Natarajan, M., and Velauthapillai, D. (2022). CO2 adsorption performance of template free zeolite A and X synthesized from rice husk ash as silicon source. *RSC Advances, 12*(36), 23221-23239. doi:10.1039/D2RA04052B

Manadee, S., Supamathanon, N., Prayoonpokarach, S., and Wittayakan, J. (2012). Catalyst preparation by addition of K and Na on zeolite NaX for transesterification of jatropha seed oil. *ACSEE, 1*, 400-412.

McCusker, L. B., and Baerlocher, C. (2001). Chapter 3 Zeolite structures. In H. van Bekkum, E. M. Flanigen, P. A. Jacobs, & J. C. Jansen (Eds.), *Studies in Surface Science and Catalysis* (Vol. 137, pp. 37-67): Elsevier.

Millward, A. R., and Yaghi, O. M. (2005). Metal–Organic Frameworks with Exceptionally High Capacity for Storage of Carbon Dioxide at Room Temperature. *Journal of the American Chemical Society, 127*(51), 17998-17999. doi:10.1021/ja0570032

Min, J. G., Kemp, K. C., and Hong, S. B. (2020). Silver ZK-5 zeolites for selective ethylene/ethane separation. *Separation and Purification Technology, 250*, 117146. doi:10.1016/j.seppur.2020.117146

Minja, R. J. A., Mbise, E., and Said, I. (2021). Potential of Using Sugarcane Leaves to Produce Pulp for Paper Making. *Journal of Textile Engineering and Fashion Technology, 3*(1), 32-35. doi:10.33140/JTEFT

Morawala, D., Dalai, A., and Maheria, K. (2019). Rice husk mediated synthesis of meso-ZSM-5 and its application in the synthesis of n-butyl levulinate. *Journal of Porous Materials, 26*(3), 677-686. doi:10.1007/s10934-018-0664-6

Moura, P. A. S., Bezerra, D. P., Vilarrasa-Garcia, E., Bastos-Neto, M., and Azevedo, D. C. S. (2016). Adsorption Equilibria of CO_2 and CH_4 in Cation-Exchanged Zeolites 13X. *Adsorption, 22*(1), 71-80. doi:10.1007/s10450-015-9738-9

Olson, D. H. (1995). The crystal structure of dehydrated NaX. *Zeolites, 15*(5), 439-443. doi:10.1016/0144-2449(95)00029-6

Pluth, J. J., and Smith, J. V. (1980). Accurate redetermination of crystal structure of dehydrated zeolite A. Absence of near zero coordination of sodium. Refinement of silicon,aluminum-ordered superstructure. *Journal of the American Chemical Society, 102*(14), 4704-4708. doi:10.1021/ja00534a024

Rainey, T., and Covey, G. (2016). Pulp and paper production from sugarcane bagasse. In (pp. 259-280).

Rani, S., Singh, A., and Kashyap, P. (2018). Pulp and Paper Making from Grass Fibre. *International Journal of Emerging Technologies and Innovative Research, 5*(8), 521-523.

Rongchapo, W., Keawkumay, C., Osakoo, N., Deekamwong, K., Chanlek, N., Prayoonpokarach, S., and Wittayakun, J. (2017). Comprehension of paraquat adsorption on faujasite zeolite X and Y in sodium form. *Adsorption Science & Technology, 36*(1-2), 684-693. doi:10.1177/0263617417715394

Roy, S., Philip, F. A., Oliveira, E. F., Singh, G., Joseph, S., Yadav, R. M., Adumbumkulath, A., Hassan, S., Khater, A., Wu, X., Bollini, P., Vinu, A., Shimizu, G., Ajayan, P. M., Kibria, M. G., and Rahman, M. M. (2023). Functional wood for carbon dioxide capture. *Cell Reports Physical Science, 4*(2), 101269. doi:10.1016/j.xcrp.2023.101269

Schlumberger, C., and Thommes, M. (2021). Characterization of Hierarchically Ordered Porous Materials by Physisorption and Mercury Porosimetry—A Tutorial Review. *Advanced Materials Interfaces, 8*(4), 2002181. doi:10.1002/admi.202002181

Seymour, G. B., Østergaard, L., Chapman, N. H., Knapp, S., and Martin, C. (2013). Fruit Development and Ripening. *Annual Review of Plant Biology, 64*(Volume 64, 2013), 219-241. doi:10.1146/annurev-arplant-050312-120057

Sharma, P., Kaur, A., Batish, D. R., Kaur, S., and Chauhan, B. S. (2022). Critical Insights Into the Ecological and Invasive Attributes of Leucaena leucocephala, a Tropical Agroforestry Species. *Frontiers in Agronomy, 4*. doi:10.3389/fagro.2022.890992

Tawachkultanadilok, P., Osakoo, N., Keawkumay, C., Deekamwong, K., Sosa, N., Rojviriya, C., Nijpanich, S., Chanlek, N., Prayoonpokarach, S., and Wittayakun, J. (2023). Synthesis and characterization of zeolite NaY dispersed on bamboo wood. *Materials, 16*(14). doi:10.3390/ma16144946

Tawachkultanadilok, P., Wittayakun, J., Valentini, F., Föttinger, K., Deekamwong, K., and Prayoonpokarach, S. (2024). Comparison of micron- and nano-sized zeolite NaY composited with bamboo charcoal and their application in CO_2 adsorption. *Materials Letters, 377*, 137511. doi:10.1016/j.matlet.2024.137511

Tepamat, T., Mongkolkachit, C., and Wasanapiarnpong, T. (2013). Synthesis of zeolite NaA and activated carbon composite from rice husk. *Suranaree J. Sci. Technol, 21*.

Valtchev, V. P., Smaihi, M., Faust, A.-C., and Vidal, L. (2004a). Dual templating function of Equisetum arvense in the preparation of zeolite macrostructures. In E. van Steen, I. M. Claeys, & L. H. Callanan (Eds.), *Studies in Surface Science and Catalysis* (Vol. 154, pp. 588-592): Elsevier.

Valtchev, V. P., Smaihi, M., Faust, A.-C., and Vidal, L. (2004b). Equisetum arvense templating of zeolite beta macrostructures with hierarchical porosity. *Chemistry of Materials, 16*(7), 1350-1355. doi:10.1021/cm035100t

Vermeiren, L., Devlieghere, F., van Beest, M., de Kruijf, N., and Debevere, J. (1999). Developments in the active packaging of foods. *Trends in food science & technology, 10*(3), 77-86.

Wang, Y., Du, T., Jia, H., Qiu, Z., and Song, Y. (2018). Synthesis, characterization and CO_2 adsorption of NaA, NaX and NaZSM-5 from rice husk ash. *Solid State Sciences, 86*, 24-33. doi:10.1016/j.solidstatesciences.2018.10.003

Wijitkosum, S. (2023). Repurposing disposable bamboo chopsticks waste as biochar for agronomical application. *Energies, 16*(2). doi:10.3390/en16020771

Wutisatwongkul, J., Thavarungkul, N., Tiansuwan, J., and Termsuksawad, P. (2016). Influence of Soda pulping variables on properties of pineapple (Ananas comosus Merr.) leaf pulp and paper studied by face-centered composite experimental design. *Advances in Materials Science and Engineering, 2016*(1), 8915362. doi:10.1155/2016/8915362

Yang, S.-T., Kim, J., and Ahn, W.-S. (2010). CO_2 adsorption over ion-exchanged zeolite beta with alkali and alkaline earth metal ions. *Microporous and Mesoporous Materials, 135*(1), 90-94. doi:10.1016/j.micromeso.2010.06.015

Zayed, M., Sallam, S., and Shetta, N. (2018). Review article on leucaena leucocephala as one of the miracle timber trees. *International Journal of Pharmacy and Pharmaceutical Sciences, 10*, 1-7. doi:10.22159/ijpps.2018v10i1.18250

CURRICULUM VITAE

Rachata Jaikla

Address E110 Suranivet 13 Dormitory, Suranaree university, 111, Maha Witthayalai Rd, Suranari, Mueang Nakhon Ratchasima District, Nakhon Ratchasima 30000 Email: gzaza2222@gmail.com

Education

2022 B.Sc. (Chemistry) with first class honors, Suranaree University of Technology (SUT), Nakhon Ratchasima, Thailand

2022 – 2025 Student in M.Sc. program in Chemistry, SUT

Scholarship

2018 – 2022 SUT King's 84th Birthday Anniversary Scholarships

2022 – 2024 SUT Outstanding Academic Performance Scholarships